JCI The Journal of Clinical Investigation

Stromal integrin α11 regulates PDGFRβ signaling and promotes breast cancer progression

Irina Primac, … , Donald Gullberg, Agnès Noel

J Clin Invest. 2019;129(11):4609-4628. https://doi.org/10.1172/JCI125890.

Research Article | Cell biology | Oncology

Graphical abstract

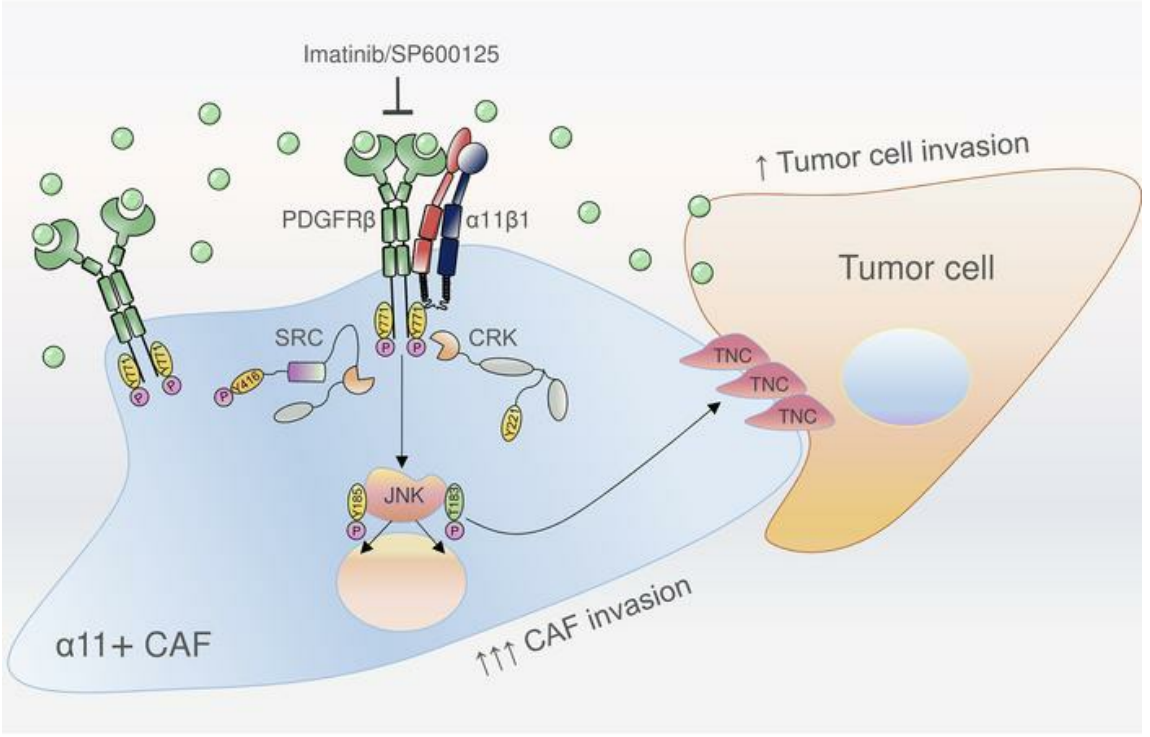

Stromal integrin α11 regulates PDGFRβ signaling and promotes breast cancer progression

Irina Primac,[1] Erik Maquoi,[1] Silvia Blacher,[1] Ritva Heljasvaara,[2,3] Jan Van Deun,[4] Hilde Y.H. Smeland,[3] Annalisa Canale,[1] Thomas Louis,[1] Linda Stuhr,[3] Nor Eddine Sounni,[1] Didier Cataldo,[1] Taina Pihlajaniemi,[2] Christel Pequeux,[1] Olivier De Wever,[4] Donald Gullberg,[3] and Agnès Noel[1]

[1]Laboratory of Tumor and Development Biology, GIGA-Cancer, University of Liège, Liège, Belgium. [2]Oulu Centre for Cell–Extracellular Matrix Research and Biocenter Oulu, Faculty of Biochemistry and Molecular Medicine, University of Oulu, Oulu, Finland. [3]Department of Biomedicine and Centre for Cancer Biomarkers (CCBIO), Norwegian Centre of Excellence, University of Bergen, Bergen, Norway. [4]Laboratory of Experimental Cancer Research, Department of Human Structure and Repair, Ghent University, Ghent, Belgium.

Cancer-associated fibroblasts (CAFs) are key actors in modulating the progression of many solid tumors, such as breast cancer (BC). Herein, we identify an integrin α11/PDGFRβ–positive CAF subset displaying tumor-promoting features in BC. In the preclinical MMTV-PyMT mouse model, integrin α11 deficiency led to a drastic reduction of tumor progression and metastasis. A clear association between integrin α11 and PDGFRβ was found at both transcriptional and histological levels in BC specimens. High stromal integrin α11/PDGFRβ expression was associated with high grades and poorer clinical outcome in human BC patients. Functional assays using 5 CAF subpopulations (1 murine, 4 human) revealed that integrin α11 promotes CAF invasion and CAF-induced tumor cell invasion upon PDGF-BB stimulation. Mechanistically, the proinvasive activity of integrin α11 relies on its ability to interact with PDGFRβ in a ligand-dependent manner and to promote its downstream JNK activation, leading to the production of tenascin C, a proinvasive matricellular protein. Pharmacological inhibition of PDGFRβ and JNK impaired tumor cell invasion induced by integrin α11$^+$ CAFs. Collectively, our study uncovers an integrin α11$^+$ subset of protumoral CAFs that exploits the PDGFRβ/JNK signaling axis to promote tumor invasiveness in BC.

Introduction

Breast cancer (BC) is the most common type of cancer and the second leading cause of cancer-related death in women worldwide. Despite increasing knowledge of BC biology and huge progress in early detection, approximately 30% of patients with early-stage BC experience disease recurrence (1). Development and progression of cancer are intimately regulated by an evolving crosstalk between tumor cells and surrounding stromal cells, which are composed of immune/inflammatory cells, endothelial cells, pericytes, and cancer-associated fibroblasts (CAFs) (2).

CAFs comprise a very heterogeneous cell population derived from different cellular sources, including resident fibroblasts, bone marrow–derived progenitor cells, adult mesenchymal stem cells, epithelial and endothelial cells, pericytes, and preadipocytes (3–5). Because of the heterogeneity of CAFs, there is no single molecular marker defining those fibroblastic cells. The most common marker, α-smooth muscle actin (αSMA), is used to define the activated state of fibroblasts, also known as "myofibroblasts," although recent data from fibrosis models suggest that αSMA is an inconsistent marker of activated fibroblasts (6). Other molecules such as fibroblast-activating protein (FAP), fibroblast-specific protein 1 (FSP1), platelet-derived growth factor receptors (PDGFRs), and neural/glial antigen 2 (NG2) are also considered as CAF markers, but they are neither exclusively specific for this cell type, nor expressed by all CAFs (7, 8). CAFs have been shown to contribute to most of the hallmarks of cancer (9). Classically, protumorigenic effects leading to increased tumor growth, invasion, and metastasis are assigned to CAFs. Those direct or indirect effects are related, at least, to their capacity to produce growth factors (5), to promote angiogenesis (10), inflammation (11), and immune response (12), to regulate metabolic reprogramming (13), and to contribute to the remodeling and mechanotransduction of the extracellular matrix (ECM) (14). Although there is mounting evidence that CAFs are good targets for new anticancer therapies (5, 15), recent studies reported tumor-inhibitory effects of CAFs on tumor progression. Indeed, the genetic depletion of αSMA$^+$ CAFs in preclinical models of pancreatic cancer led, surprisingly, to increased tumor growth rather than to an expected reduced cancer progression (16, 17). Altogether, these data highlight CAF heterogeneity, not only in terms of cellular sources and biomarkers, but also in their capacity to promote or inhibit tumor progression. Identifying molecular determinants of functionally distinct CAF subsets is therefore critical to elucidate the contrasting biological actions of these stromal cells during cancer progression.

Tumor- and stroma-derived PDGFs (PDGF-AA, PDGF-BB, PDGF-AB, PDGF-CC, and PDGF-DD) signal by binding to their tyrosine kinase receptors (PDGFRα and PDGFRβ) and play a key role in the recruitment and phenotypic features of CAFs that infiltrate BCs (18–20). PDGFs initiate the desmoplastic reaction,

Conflict of interest: DG is named as an inventor on a patent application relating to the Mab203E1H5 (EP18155716) antibody filed by the University of Bergen.

Submitted: November 5, 2018; **Accepted:** June 24, 2019; **Published:** September 23, 2019.
Reference information: *J Clin Invest*. 2019;129(11):4609–4628.
https://doi.org/10.1172/JCI125890.

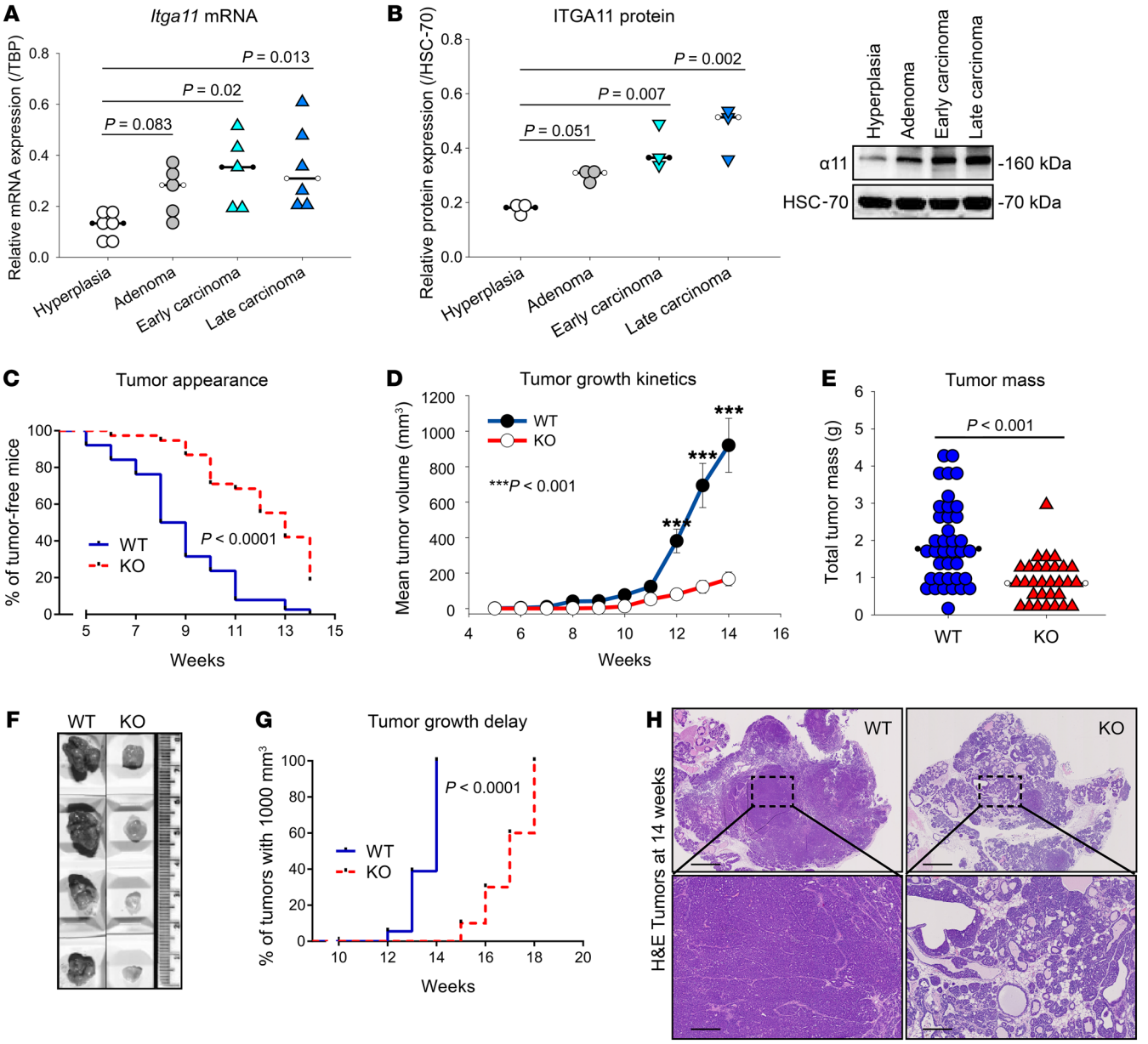

Figure 1. High integrin α11 expression associates with tumor progression in PyMT mouse breast tumor model. PyMT breast tumors analyzed at different stages: hyperplasia, adenoma, early carcinoma, and late carcinoma (5, 7, 10, and 14 weeks, respectively). (**A**) Quantitative reverse transcriptase PCR of *Itga11* mRNA levels. Median of 5–6 tumors normalized to TBP. One-way ANOVA with Holm-Šidák multiple-comparisons test. (**B**) Western blot of ITGA11 protein levels. Median of 3 tumors normalized to HSC-70. One-way ANOVA with Holm-Šidák multiple-comparisons test. (**C**) Kaplan-Meier plot showing the appearance of palpable tumors in PyMT *Itga11*$^{+/+}$ (WT) (n = 19) and *Itga11*$^{-/-}$ (KO) mice (n = 19). Log-rank (Mantel-Cox) test. (**D**) Tumor growth kinetics (n = 19 WT, n = 19 KO mice, 2 tumors per mouse). Two-way ANOVA test with Holm-Šidák multiple-comparisons test. (**E**) Tumor mass at 14 weeks. Median of tumor mass (n = 38 WT, n = 30 KO tumors). Mann-Whitney test. (**F**) Representative pictures of tumors at sacrifice. (**G**) Kaplan-Meier plot showing tumor growth delay in KO mice. Data are presented as the percentage of WT (n = 19) and KO (n = 29) mice reaching 1000 mm^3 of tumor volume. Log-rank (Mantel-Cox) test. (**H**) Representative images of H&E staining of tumors. Scale bars: 2 mm (original); 0.5 mm (zoom). ***P < 0.001.

stimulate angiogenesis, and promote tumor growth and metastatic dissemination (21). PDGF signaling in CAFs has been shown to act as a determinant of the molecular subtype in BC (18). Previous studies have also reported that PDGFRβ expression in fibroblasts of BC patients is associated with aggressiveness, poor prognosis, and altered therapeutic response (22, 23). PDGFRβ signaling is regulated not only by growth factors but also by a functional interplay with integrins (24–26). Recently, integrin α11 (ITGA11), a collagen-binding mesenchymal integrin, emerged as a novel CAF marker (27). The expression of this integrin is correlated with myofibroblast differentiation, matrix reorganization, and collagen deposition (28–30). While integrin α11 function in wound healing has been well described (31), only a very limited number of reports have assessed its role in cancer. In lung cancer, stromal integrin α11 has been reported to increase the tumorigenicity of cancer cells by regulating IGF-2 production (32) and matrix stiffness (33).

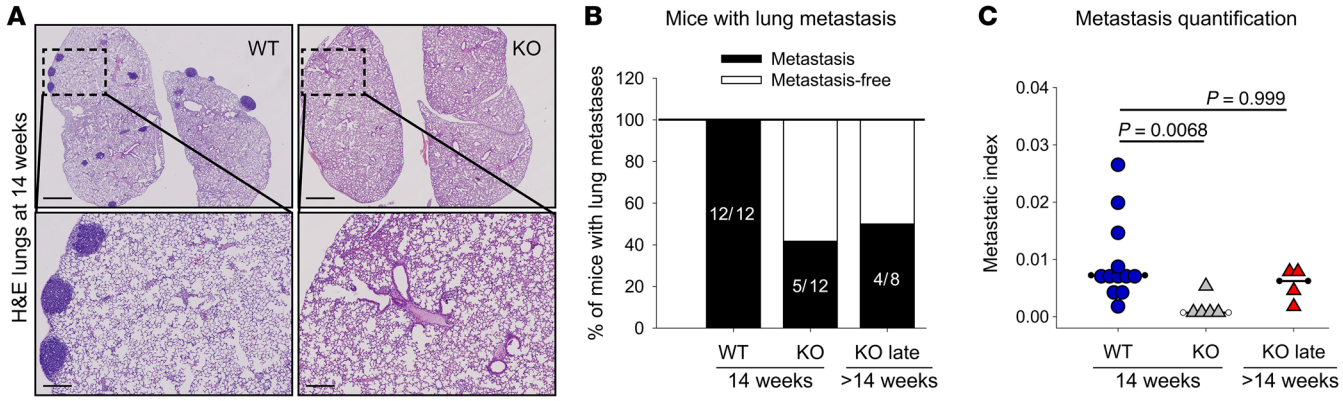

Figure 2. High integrin α11 expression associates with metastasis. (**A**) Representative images of H&E staining of lungs issued from PyMT WT and KO mice. Scale bars: 1 mm (original); 250 μm (zoom). (**B** and **C**) Lung metastasis in mice at sacrifice (14 weeks for WT and KO groups and when tumors reached a 1000-mm^3 volume for the "KO late" group). Results are expressed as percentage of mice with lung metastasis (**B**) and median of metastatic index (lung tumor area/total lung area) analyzed in mice bearing metastasis (**C**); n = 12 (WT); n = 5 (KO); n = 4 (KO late). One-way ANOVA with Dunn's multiple-comparisons test.

The contribution of integrin α11 in BC progression and its cross-talk with the surrounding tyrosine kinase receptors has not been yet documented. Prompted by findings of prominent integrin α11 expression in human BCs, we set out to identify the subset of CAFs expressing integrin α11, to investigate its contribution to BC growth and invasion in vitro and in vivo, and to molecularly define its role in CAF functions.

Results

Genetic Itga11 ablation in mice delays tumor growth and drastically reduces metastasis. We used the transgenic polyoma middle T oncogene–induced (PyMT-induced) mouse model (FVB/N genetic background), which accurately reproduces the stepwise progression of human BC with high metastatic dissemination to lungs (34). This model was also chosen for its high content of desmoplasia and infiltrating stromal cells, particularly fibroblasts at all stages of tumor progression. We first assessed integrin α11 expression, at both the mRNA and the protein level, at different time points of PyMT primary tumor development. A progressive increase of α11 expression was evidenced from hyperplastic nodules (5 weeks) to carcinoma tumors (10–14 weeks) (Figure 1, A and B). *Itga11*-deficient mice (*Itga11*$^{-/-}$ FVB/N genetic background) were crossed with PyMT mice, resulting in 2 groups of female mice, hemizygous for PyMT transgene: PyMT *Itga11*$^{+/+}$ (WT) and PyMT *Itga11*$^{-/-}$ (KO). Phenotypically, *Itga11*-deficient mice show dwarfism, increased mortality, and defective incisors (35) that were maintained in the generated PyMT *Itga11*-KO mice. *Itga11* genetic ablation led to a significant delay in the appearance of palpable tumors (Figure 1C) and reduction of tumor growth (Figure 1, D and E). The average time for tumor appearance in 50% of mice was 8 weeks in WT mice and 12 weeks in KO mice (Figure 1C). Tumor volume at sacrifice (week 14) was reduced more than 5-fold (Figure 1, D–F) in KO PyMT mice compared with WT PyMT mice. A tumor growth delay of about 3 weeks was observed between the 2 genotypes when a group of KO PyMT mice was left for longer than 14 weeks ("KO late"), until tumors reached a volume of 1000 mm^3 as observed in WT mice at 14 weeks (Figure 1G). This group was monitored until week 18. WT PyMT tumors were characterized by large and dense tumor lobules with high collagen content (Figure 1H and Supplemental Figure 1, A and B; supplemental material available online with this article; https://doi.org/10.1172/JCI125890DS1). In contrast, KO PyMT tumors were composed of small lobules intermingled with adipose tissue and less collagen deposition (Figure 1H and Supplemental Figure 1, A and B). Strikingly, *Itga11* deficiency dramatically reduced metastasis formation (Figure 2, A–C). At week 14, a twice-lower incidence of pulmonary metastases was seen in KO mice (40% of KO mice vs. 100% of WT mice) (Figure 2B). Importantly, such defect in lung metastasis incidence was still pronounced at later time points (KO late group: >14 weeks) when tumors reached a volume of 1000 mm^3 (Figure 2, B and C). Note that only KO and KO late mice with metastasis (5 of 12 and 4 of 8 mice, respectively) were taken into account for metastatic index determination (Figure 2C).

Integrin α11 defines a subset of PDGFRβ$^+$ CAFs. Immunohistochemical (IHC) stainings were conducted on primary PyMT tumors at different stages (Figure 3A). Anti-α11 antibody specificity was assessed using *Itga11*-deficient PyMT tumors (Figure 3A). Integrin α11 positivity was easily detected at week 10 and intense at week 14 (Figure 3A). As expected, integrin α11 staining was mostly restricted to the stromal compartment, confirmed also by the absence of association with pan-cytokeratin (Supplemental Figure 1C). Remarkably, integrin α11 strongly colocalized with PDGFRβ and was poorly associated with other stromal markers such as αSMA, PDGFRα, NG2 (Figure 3A), FAP, or FSP1 (Supplemental Figure 1D). Notably, PDGFRβ staining was concomitantly detected in early tumors with NG2 (weeks 5 and 7), a pericyte marker (Figure 3A). A computerized quantification revealed that 60% of total α11$^+$ cells were positive for PDGFRβ, while a low proportion of these cells were also positive for another marker: PDGFRα (<9%), αSMA (<9%), FAP (<23%), FSP1 (<6%), or NG2 (<12%) (Figure 3A and Supplemental Figure 1D). Thus, integrin α11 is mainly expressed by PDGFRβ$^+$ CAFs. Accordingly, higher levels of PDGFRβ mRNAs (Figure 3B) and proteins (Figure 3C) were detected in PyMT tumors compared with hyperplastic tissues. In sharp contrast to its counterpart isoform, PDGFRα expression was

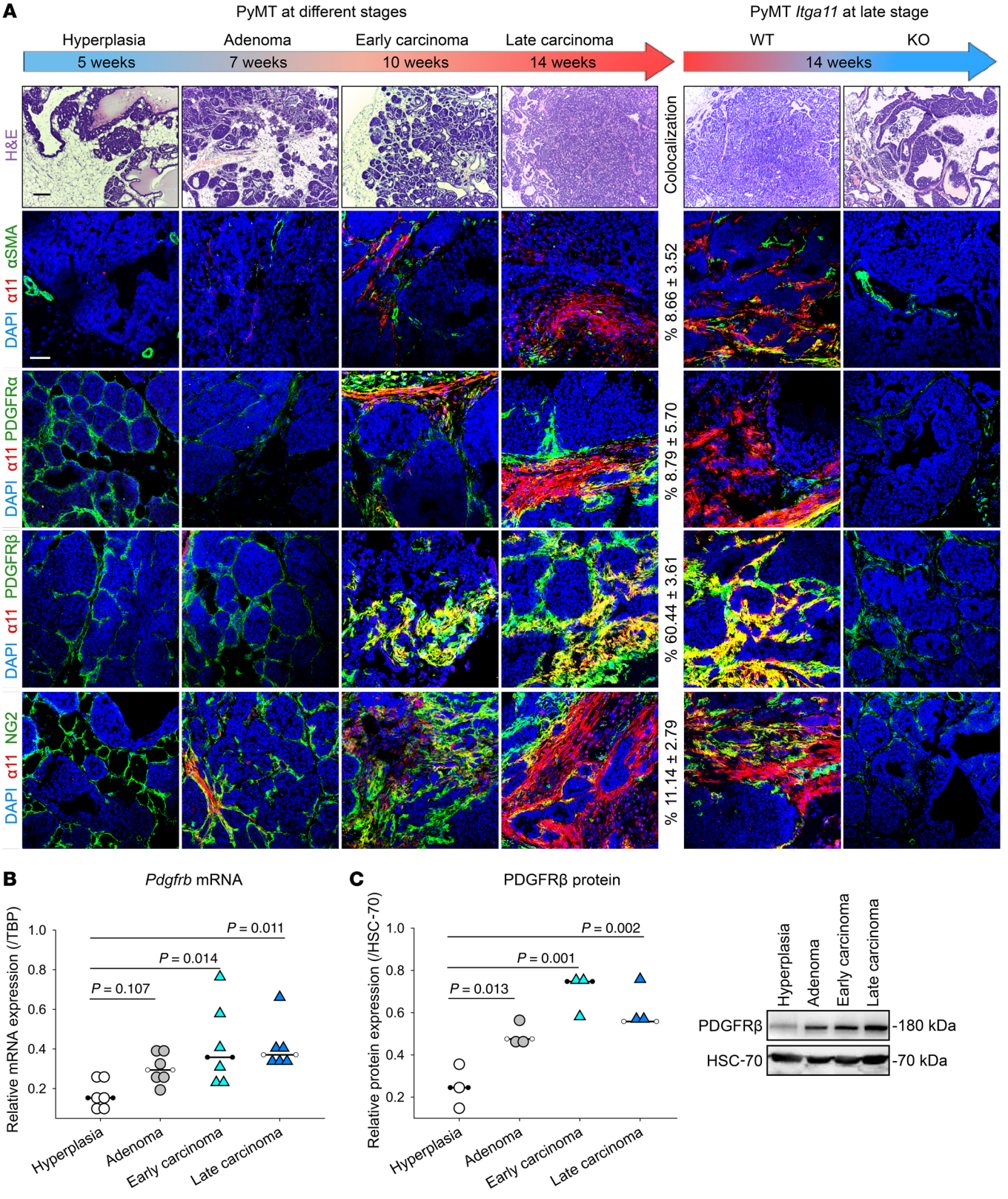

Figure 3. Integrin α11 defines a PDGFRβ⁺ CAF subpopulation, and its expression is increased during tumor progression. (**A**) Representative pictures of H&E and immunofluorescence staining of PyMT mice at different stages (left panel) and PyMT *Itga11*-WT and -KO mice at late stage (14 weeks) (right panel). Immunofluorescence confocal pictures show the costaining of integrin α11 (red) and αSMA, PDGFRα, or PDGFRβ (green). Nuclei stained with DAPI (blue). Scale bars: 50 μm. The percentages of cells positive for integrin α11 and a second marker compared with the total number of α11⁺ cells are indicated ("Colocalization"). Colocalization was determined by a computerized method on more than 12 stromal fields per tumor (n = 8 for each genotype). (**B** and **C**) Quantification of *Pdgfrb* mRNA levels (quantitative reverse transcriptase PCR, data normalized to TBP) (n = 6) (**B**) and protein levels (Western blot, data normalized to HSC-70) (n = 3) (**C**) in PyMT tumors. Representative pictures of Western blots are shown in the right panel. One-way ANOVA with Holm-Šidák multiple-comparisons test.

poorly modulated during PyMT tumor progression and not related to integrin α11 expression (Supplemental Figure 1, E and F).

To determine whether tumor-resident CAFs or other host integrin α11$^+$ cells are responsible for the observed phenotype, *Itga11*-WT PyMT tumors were engrafted into *Itga11*-WT and -KO receiver mice (Supplemental Figure 2A). Similar tumor growth and mass (Supplemental Figure 2, A–C) were observed in both receiver mice. Histologically, transplanted tumors showed indistinguishable large and invasive tumor lobules (Supplemental Figure 2D) with strong stromal integrin α11/PDGFRβ expression (Supplemental Figure 2E). This demonstrates that integrin α11$^+$ resident CAFs are sufficient to promote tumor progression in an environment proficient or deficient in *Itga11*.

ITGA11 expression is increased in human BCs. To determine whether integrin α11 expression is altered in human BC, a meta-analysis of publicly available gene expression data using the Oncomine database was performed. We compared *ITGA11* expression in 2415 BC versus 261 normal adjacent BC samples from 8 data sets. *ITGA11* was found overexpressed in BC samples (gene median rank 2476.0, $P = 1.92 \times 10^{-10}$) in 7 of the 8 data sets included in the meta-analysis (Figure 4A and Supplemental Table 1). Further analyses showed increased *ITGA11* mRNA levels in BC samples including invasive ductal BC (Figure 4, B–D, G and H), invasive lobular BC (Figure 4B), invasive BC (Figure 4, B, E, and F), ductal BC in situ (Figure 4D), tubular BC (Figure 4C), and mixed lobular and ductal BC (Figure 4B) as compared with the corresponding normal breast tissues ($P < 0.05$). The high variance of *ITGA11* expression observed in some tumor groups might result from interindividual and intratumoral heterogeneities.

Oncomine analysis of additional cancer data sets confirmed *ITGA11* overexpression in several types of cancer relative to matched normal tissue, including lung, pancreas, colorectal, and gastric cancers (Supplemental Figure 3).

In addition, Kaplan-Meier analysis of BC patients stratified by *ITGA11* mRNA levels showed that high *ITGA11* mRNA levels (probe 23335_at) were correlated with lower overall (Figure 4I) and distant metastasis–free (Figure 4J) survival than were low *ITGA11* mRNA levels. Similar results were obtained with 2 other *ITGA11* probes (222899_at and 1554819_a_at). Collectively, these in silico data suggest that increased *ITGA11* mRNA levels observed in human BC associate with a worse prognosis.

ITGA11 expression correlates with a stromal gene signature in human BC. Given the stromal integrin α11 expression, we used Gene Expression Omnibus (GEO) microarray data sets to analyze the global gene expression in microdissected human BC specimens: GSE14548, GSE33692, GSE41228 (36), and GSE68744 (Figure 5, A–D). Elevated *ITGA11* expression was found in the stromal compartment as compared with the epithelia of both ductal carcinoma in situ (DCIS) and invasive ductal carcinoma (IDC)/invasive breast carcinoma (Figure 5, A–D). Furthermore, microarray data sets (GSE8977, GSE9014, and GSE14548) comparing stroma microdissected from normal breast and BC samples unveiled a significantly increased *ITGA11* expression in cancerous stroma (Supplemental Figure 4, A–C).

Next, we searched for genes whose expression profile was best correlated (Pearson's correlation coefficient > 0.5) to *ITGA11* mRNA levels in BC samples. Data mining was conducted in 3 BC cohorts using cBioPortal (TCGA breast and METABRIC) and the bc-GenExMiner genomic tool (36 data sets including 5861 BC patients). For each cohort (TCGA, METABRIC, and GenExMiner), genes with Pearson's correlation coefficients greater than 0.5 were selected and intersected (Figure 5E and Supplemental Table 2) to produce a single list of coexpressed genes ($n = 51$) defined as the *ITGA11*-associated gene signature. Pathway enrichment analysis using the Reactome knowledgebase (37) revealed that pathways significantly (FDR Q value < 0.05) enriched in *ITGA11*-associated gene signature included at least *extracellular matrix organization*, *collagen degradation*, *integrin cell surface interactions*, and *signaling by PDGF* (Figure 5F and Supplemental Table 3).

To further characterize the cell subset expressing *ITGA11* in human BC, we correlated its mRNA expression levels with 12 genes representative of different tumor-associated cell populations. In bc-GenExMiner analysis, *ITGA11* mRNA levels poorly correlated with epithelial markers (E-cadherin/*CDH1*: Pearson's $r = 0.01$), pericyte markers (chondroitin sulfate proteoglycan NG2/*CSPG4*: $r = 0.16$), and endothelial markers (*PECAM1*: $r = 0.04$) (Figure 5G and Supplemental Figure 4D). In contrast, stronger correlations were observed with several markers of activated fibroblasts, including αSMA (*ACTA2*: $r = 0.41$), PDGFRβ (*PDGFRB*: $r = 0.47$), *FAP* ($r = 0.58$), lysyl oxidase (*LOX*: $r = 0.61$), fibrillar collagens (*COL1A1*: $r = 0.53$; *COL3A1*: $r = 0.45$; *COL5A1*: $r = 0.63$), and collagen type X (*COL10A1*: $r = 0.69$). In line with the in vivo data, *ITGA11* correlated with *PDGFRB*, but not with *PDGFRA* ($r = 0.28$). Similar results were confirmed in TCGA breast and METABRIC cohorts. In addition, the TCSBN database (38) was used to analyze the integrative coexpression landscape of integrin α11 with query genes (*CDH1*, *ACTA2*, *CSPG4*, *PDGFRA*, and *PDGFRB*) in normal and tumoral breast tissues (Supplemental Figure 5). Again, a high *ITGA11* coexpression with stromal markers was found in BC tissues compared with the normal ones. Among the neighbor genes of the *ITGA11* cluster, we found many matrix-related proteins: collagens (*COL3A1*, *COL4A2*, *COL6A3*, *COL10A1*, *COL11A1*, and *COL12A1*), fibronectin (*FN1*), thrombospondin 2 (*THBS2*), lumican (*LUM*), laminin A4 (*LAMA4*), and entactin (*NID1*), as well as functional proteins such as *NOX4*, *PDGFRB*, and *LRP1* (Supplemental Figure 5).

Integrin α11/PDGFRβ density associates with a poor outcome in human BC. We next performed double immunostaining of integrin α11 and PDGFRβ in human BC samples and the associated normal tissues of DCIS and IDC ($n = 68$ of different BC subtypes) (Figure 6A). Densities of integrin α11 or PDGFRβ were 2- to 3-fold higher in IDC tumors compared with DCIS (Figure 6, B–D). The increase in integrin α11 and PDGFRβ colocalization (percentage of positive cells per tumor area) was more pronounced in IDC versus DCIS (5-fold increase). This was particularly evident in more aggressive BC molecular subtypes (HER2 and TNBC). In line with the mouse study, more than 70% of α11$^+$ CAFs were positive for PDGFRβ and more than 60% of PDGFRβ$^+$ CAFs were positive for α11 in IDC tumors (Figure 6, E and F). This further supports the concept that integrin α11 is mainly expressed by a subpopulation of PDGFRβ$^+$ CAFs in human BC. Next, we analyzed the association between this α11/PDGFRβ–positive CAF subset and patient outcome. A positive correlation between the double α11/PDGFRβ positivity and high proliferation rate (percentage Ki67) was detect-

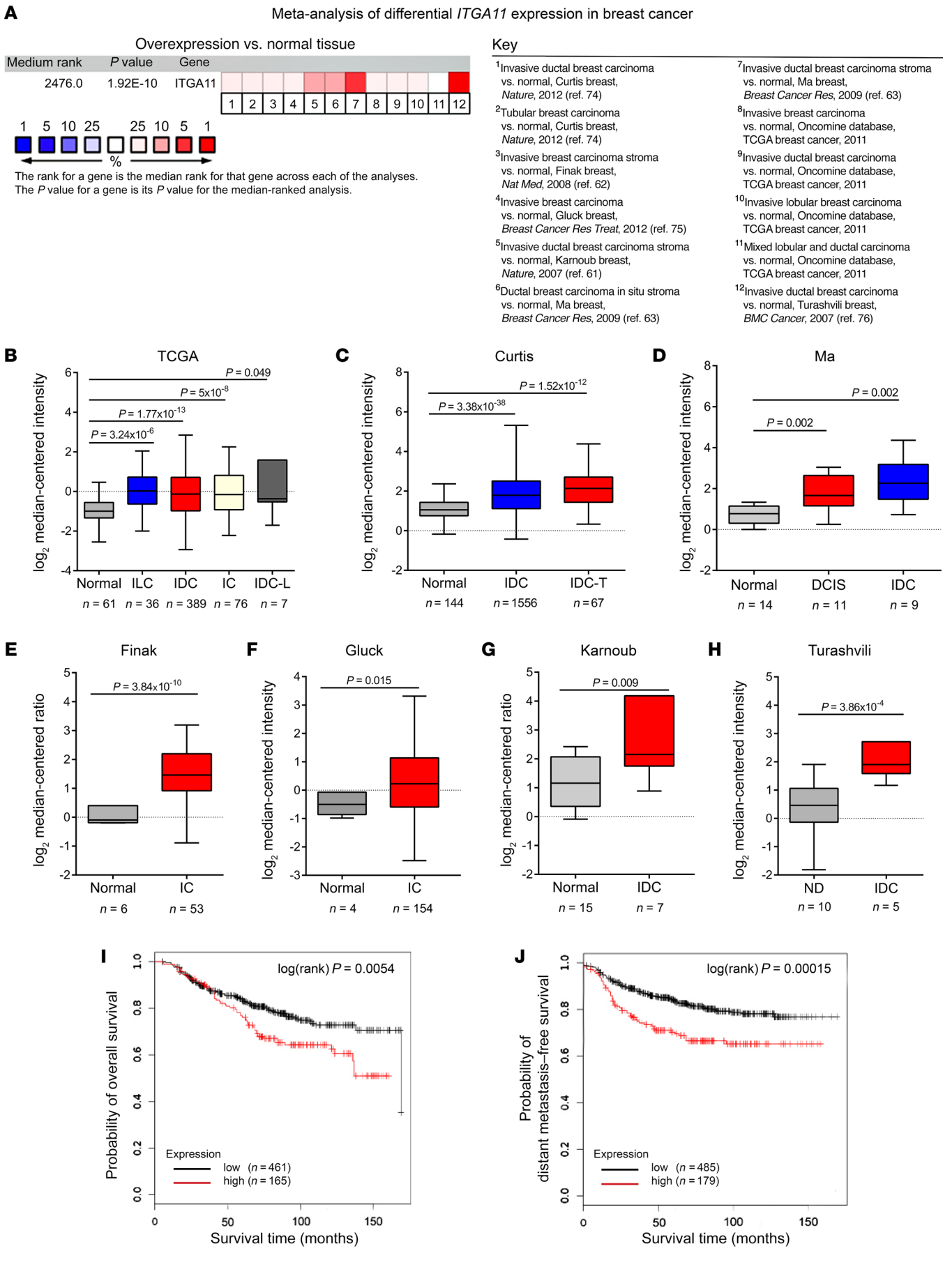
A
Meta-analysis of differential ITGA11 expression in breast cancer
Overexpression vs. normal tissue
Medium rank
P value
Gene
2476.0
1.92E-10
ITGA11
1 2 3 4 5 6 7 8 9 10 11 12
1 5 10 25 25 10 5 1
%
The rank for a gene is the median rank for that gene across each of the analyses.
The P value for a gene is its P value for the median-ranked analysis.
Key
[1]Invasive ductal breast carcinoma vs. normal, Curtis breast, Nature, 2012 (ref. 74)
[2]Tubular breast carcinoma vs. normal, Curtis breast, Nature, 2012 (ref. 74)
[3]Invasive breast carcinoma stroma vs. normal, Finak breast, Nat Med, 2008 (ref. 62)
[4]Invasive breast carcinoma vs. normal, Gluck breast, Breast Cancer Res Treat, 2012 (ref. 75)
[5]Invasive ductal breast carcinoma stroma vs. normal, Karnoub breast, Nature, 2007 (ref. 61)
[6]Ductal breast carcinoma in situ stroma vs. normal, Ma breast, Breast Cancer Res, 2009 (ref. 63)
[7]Invasive ductal breast carcinoma stroma vs. normal, Ma breast, Breast Cancer Res, 2009 (ref. 63)
[8]Invasive breast carcinoma vs. normal, Oncomine database, TCGA breast cancer, 2011
[9]Invasive ductal breast carcinoma vs. normal, Oncomine database, TCGA breast cancer, 2011
[10]Invasive lobular breast carcinoma vs. normal, Oncomine database, TCGA breast cancer, 2011
[11]Mixed lobular and ductal carcinoma vs. normal, Oncomine database, TCGA breast cancer, 2011
[12]Invasive ductal breast carcinoma vs. normal, Turashvili breast, BMC Cancer, 2007 (ref. 76)
B
TCGA
log2 median-centered intensity
P = 0.049
P = 5x10-8
P = 1.77x10-13
P = 3.24x10-6
Normal ILC IDC IC IDC-L
n = 61 n = 36 n = 389 n = 76 n = 7
C
Curtis
log2 median-centered intensity
P = 1.52x10-12
P = 3.38x10-38
Normal IDC IDC-T
n = 144 n = 1556 n = 67
D
Ma
log2 median-centered intensity
P = 0.002
P = 0.002
Normal DCIS IDC
n = 14 n = 11 n = 9
E
Finak
log2 median-centered ratio
P = 3.84x10-10
Normal IC
n = 6 n = 53
F
Gluck
log2 median-centered intensity
P = 0.015
Normal IC
n = 4 n = 154
G
Karnoub
log2 median-centered ratio
P = 0.009
Normal IDC
n = 15 n = 7
H
Turashvili
log2 median-centered intensity
P = 3.86x10-4
ND IDC
n = 10 n = 5
I
log(rank) P = 0.0054
Probability of overall survival
Expression
low (n = 461)
high (n = 165)
Survival time (months)
J
log(rank) P = 0.00015
Probability of distant metastasis–free survival
Expression
low (n = 485)
high (n = 179)
Survival time (months)

Figure 4. Integrin α11 expression is increased in human breast cancers. (**A**) Meta-analysis data of integrin α11 differential expression in BCs versus breast normal tissues. Oncomine microarray database was used to analyze *ITGA11* mRNA expression, and meta-analysis was performed on 12 analyses from 7 microarray data sets (2375 patients). Data are shown as median rank of *ITGA11* expression through each data set analysis. *P* value for *ITGA11* was determined using the median-ranked analysis of BC versus normal tissues. (**B**–**H**) Differential expressions of *ITGA11* mRNA in the 7 data sets included in the meta-analysis (Normal, normal adjacent breast tissue; IC, invasive breast carcinoma; IDC, invasive ductal breast carcinoma; IDC-L, mixed lobular and ductal breast carcinoma; IDC-T, invasive ductal breast carcinoma–tubular type; ILC, invasive lobular breast carcinoma). Median and interquartile range (10th and 90th percentiles). Two-sided *t* test for 2-class differential expression analyses and Pearson's correlation for multiclass analyses. FDR-corrected *P* values. (**I** and **J**) Kaplan-Meier plots showing the overall survival (**I**) and distant metastasis–free survival (**J**) for *ITGA11* expression (probe: 23335_at). Log-rank *P* values calculated with the Kaplan-Meier plotter website.

ed (Figure 6G). Furthermore, higher α11/PDGFRβ stromal density was associated with high tumor grade, metastasis, and patient mortality (Figure 6, H–J). The analysis of the spatial distribution of $\alpha11^+$, $PDGFR\beta^+$, and double-positive cells (Figure 6K) revealed that α11/PDGFRβ double positivity was mostly associated with juxta-epithelial fibroblasts (high frequency at short distances).

Integrin α11–expressing CAFs promote in vitro tumor cell invasion in response to PDGF-BB. The in vivo and in silico studies revealed a strong association between integrin α11 and PDGFRβ in BC stroma. We next performed Western blot analyses on several mouse and human primary cells and established cell lines: primary mouse PyMT CAFs (mCAFs) and cancer cells (PyMT), primary human breast CAFs (hCAFs), human blood (HUVEC) and lymphatic (HMVEC) endothelial cells, and MDA-MB-231, MCF-7, and SKBr3 human BC cells (Supplemental Figure 6A). Both mCAFs and hCAFs showed high integrin α11 expression levels, while other stromal and tumor cells had undetectable levels of this integrin. For functional investigations in vitro, 2 approaches were used: (a) CAFs were isolated from WT (mCAF WT) and KO (mCAF KO) PyMT late carcinomas; and (b) ITGA11 expression was downregulated (knockdown [KD]) in WT CAFs issued from PyMT tumors or human BC CAFs through siRNA technology (mCAF/hCAF CTRL and KD). The overall efficiency of integrin knockdown was greater than 80% (Supplemental Figure 6B). Those different CAF populations were tested for their ability to remodel a collagen matrix and promote cell invasion (Figure 7, A–F, and Supplemental Figure 6, C–H). While WT CAFs contracted the collagen lattice to >80% of its original size, KO mCAFs achieved less than 60% of gel reduction within 96 hours (Supplemental Figure 6C). Similarly, α11-silenced CAFs (mCAFs and hCAF1 KD) displayed impaired collagen contraction capacity (70% in CTRL mCAF/hCAF1 vs. 40% in mCAF KD and 50% in hCAF1 KD) (Supplemental Figure 6, D and E). Next, we evaluated the impact of integrin α11 on CAF invasion in spheroids embedded in a 3D collagen matrix, a model implying ECM remodeling by proteases. Integrin α11 deficiency impaired CAF invasion into the matrix under basal conditions (Control) (Figure 7, A–C). Interestingly, when stimulated with PDGF-BB, the main ligand of PDGFRβ, mCAFs and hCAF1 showed a strong increase in CAF invasion with a higher degree of response to PDGF-BB for $\alpha11^+$ CAFs compared with deficient ones (Figure 7, A–C). These data suggest that $\alpha11^-$ CAFs are less sensitive to PDGF-BB stimulation than their WT counterpart. These findings were confirmed with 3 other primary hCAFs (hCAF2–4) issued from hormone-positive or TNBC BC patients (Supplemental Figure 7, A–C).

We next evaluated the impact of integrin $\alpha11^+$ CAFs on tumor cell invasion upon PDGF-BB stimulation. To address the heterogeneity issues, CAFs were coculture with tumor cells with distinct molecular and invasive properties: mCAFs with PyMT tumor cells (low hormone sensitivity, more invasive) (Figure 7D) or hCAF1–4 with MCF-7 (high hormone sensitivity, less invasive) and MDA-MB-231 cells (hormone insensitivity, more invasive) (Figure 7, E and F, and Supplemental Figure 7, D–I). As previously seen in CAF homospheroids, $\alpha11^+$ CAFs in heterospheroids were more invasive than α11-deficient ones (Supplemental Figure 6F). Tumor cell coculture with CAFs in heterospheroids resulted in increased tumor cell invasion as compared with that observed in homospheroids. Moreover, integrin $\alpha11^+$ CAFs had a higher capacity to promote tumor cell invasion than α11-deficient CAFs (Figure 7, D–F, and Supplemental Figure 6G). Importantly, PDGF-BB treatment strongly enhanced tumor cell invasion when tumor cells were cocultured with $\alpha11^+$ CAFs (Figure 7, D–F, and Supplemental Figure 6G), but not to α11-deficient CAFs. These data point to the incapacity of α11-deficient CAFs to promote tumor cell invasiveness via PDGF signaling. Notably, while CAFs were sensitive to PDGF-BB stimulation (Figure 7, A–C), tumor cell invasion was not affected by PDGF-BB treatment in homospheroids (Figure 7, D–F). The invasive promoting effects of CAFs were comparable for all tumor cell types (2 human and 1 murine) and CAFs used (4 human and 1 murine) (Figure 7 and Supplemental Figure 7, D–I).

To investigate whether CAF-derived integrin α11 promotes tumor cell invasion by a direct cell-cell contact or through soluble factor production, we analyzed tumor cell invasion in homospheroids treated with conditioned medium derived from WT or KO CAFs prestimulated or not with PDGF-BB (Supplemental Figure 6H). CAF-derived conditioned medium did not improve tumor cell invasion in the absence or the presence of PDGF-BB for both WT and KO CAFs. Thus, $\alpha11^+$ CAFs require cell-cell contacts or a juxtaposition to tumor cells to promote their invasion.

Integrin α11 promotes the activation of PDGFRβ and JNK downstream signaling. For mechanistic investigation, we evaluated the impact of integrin α11 on PDGFRβ activation and its downstream signaling. We first determined whether integrin α11 takes part in a molecular complex with PDGFRβ by coimmunoprecipitation (Figure 8A). While no α11/PDGFRβ complex was detected under basal conditions, a complex was formed within 5 minutes, peaked at 10 minutes, and persisted until 60 minutes upon PDGF-BB stimulation of WT CAFs. Given the key role of CrkII (herein named CRK) as a connector between tyrosine kinase receptors (RTKs), integrins, and downstream effectors (39, 40), we searched for CRK in immunoprecipitates. In WT CAFs, a ligand-dependent recruitment of CRK in the complex formed with PDGFRβ was detected 5 minutes after stimulation and maintained concomitantly with the presence of integrin α11. In sharp contrast, the association of CRK in a molecular complex with PDGFRβ was reduced and transient (until 30 minutes) in KO CAFs, while the total amount of CRK protein was not modulated in comparison with the WT condition

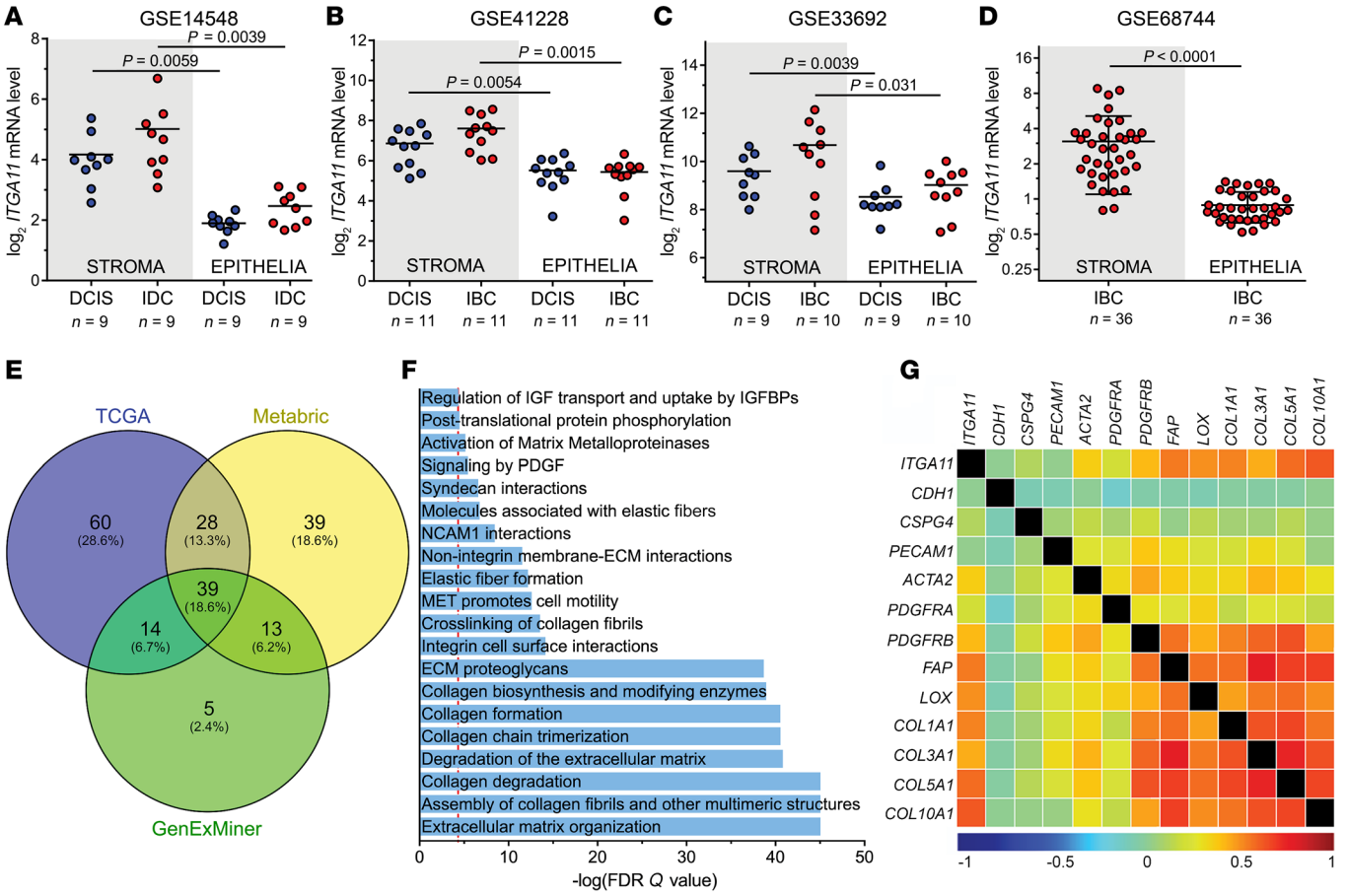

Figure 5. Integrin α11 expression correlates with a stromal gene signature in human BC. (**A**–**D**) *ITGA11* mRNA expression in microdissected stromal and epithelial compartments from ductal carcinoma in situ (DCIS) and invasive ductal (IDC)/invasive breast (IBC) carcinoma issued from GSE14548 (**A**), GSE41228 (**B**), GSE33692 (**C**), and GSE68744 (**D**) data sets. The $\log_2$-transformed *ITGA11* expression values were exported from GEO2R and analyzed in GraphPad Prism. Significance was assessed by paired 2-tailed *t* test (normal distribution) and Wilcoxon matched-pairs signed-rank test (non-normal distribution). (**E**) Venn diagram depicting the overlap and number of genes associated with *ITGA11* expression in BC across 3 genomic data sets (TCGA, METABRIC, and GenExMiner). (**F**) Reactome pathway-enriched analysis showing biological processes and pathways correlated with *ITGA11*-associated gene signature (top 20 significant pathways). Red dotted line, FDR-adjusted *Q* value = 0.05. (**G**) Targeted heat matrix showing correlation between *ITGA11* and 12 selected genes representing different tumor-associated cell populations. Data mining was performed using bc-GenExMiner 4.1. Color scale depicts Pearson's correlation coefficients from –1 (dark blue, strong negative correlation) to +1 (dark red, strong positive correlation).

(Figure 8A). Immunofluorescence staining on CAFs revealed integrin α11 clustering at focal adhesions in the absence or presence of PDGF-BB stimulation. Under basal conditions, PDGFRβ showed a diffuse distribution within WT and KO CAFs, while it colocalized within α11$^+$ focal adhesions upon PDGF-BB stimulation. KO CAFs displayed diffuse and less organized PDGFRβ staining at the cell surface, even after PDGF-BB treatment (Figure 8B).

We next evaluated integrin α11 implication in PDGFRβ activation and downstream mediator phosphorylation (Figure 9, A and B). In WT CAFs, a robust PDGFRβ phosphorylation was detected after PDGF-BB stimulation, peaking from 5 minutes to 30 minutes and then gradually decreasing by 60 minutes (Figure 9, A and B). The highest difference in PDGFRβ phosphorylation between WT and KO CAFs was seen with Y771, while the classical Y751 residue was not affected by α11 deficiency (Figure 9A and Supplemental Figure 8A). Accordingly, no difference was detected in AKT, ERK, or PLCG1 phosphorylation between the two CAF genotypes (Supplemental Figure 8A). A drastic reduction of JNK and SRC phosphorylation was detected in KO cells (Figure 9, A and B). Given CRK interaction with PDGFRβ (Figure 8A), we investigated the phosphorylation of this adaptor molecule at the Y221 residue, a negative regulatory site of protein activity (41). Upon PDGF-BB stimulation, CRK was phosphorylated at Y221 in both WT and KO cells, confirming its recruitment by the receptor. Interestingly, CRK inactivation through Y221 phosphorylation and intramolecular folding was more pronounced in KO CAFs, suggesting a reduced CRK activation (Figure 9, A and B). To exclude the implication of PDGFRα, another partner of the CRK molecule, we investigated PDGFRα phosphorylation at the Y762 residue, the docking site for CRK (42). Upon PDGF-BB stimulation, no increase in Y762 phosphorylation was seen, excluding PDGFRα implication in CRK activation in these cells (Supplemental Figure 8B).

The direct contribution of PDGFRβ in CRK, SRC, and JNK phosphorylation in WT cells is further supported by the pharmacological blockade of their phosphorylation with imatinib, an inhibitor of PDGFRβ kinase activity (Figure 9C and Supplemental Figure 8C). We next investigated a target of PDGFRβ and JNK signaling, the proinvasive matricellular protein tenascin C (43,

44). Under basal conditions, a high amount of tenascin C was produced by WT CAFs, which was strongly promoted by PDGF-BB (Figure 9, D and E). Conversely, KO CAFs produced a low amount of tenascin C (Figure 9D), even after PDGF-BB stimulation (Figure 9E). Pharmacological inhibition of PDGFRβ and JNK signaling abolished PDGF-BB–induced tenascin C expression in WT CAFs, without affecting KO CAFs (Figure 9E). To further confirm the relevance of tenascin C, we analyzed human BC samples for a triple colocalization (Figure 10, A–C). Tenascin C, α11, and PDGFRβ were strongly coexpressed, particularly in IDC tumors when compared with normal associated tissues and DCIS (Figure 10A). Tenascin C expression was strongly correlated with the double receptor colocalization, particularly in IDC HER2 and TNBC subtypes (Figure 10B). Furthermore, we measured the mean distance separating extracellular tenascin C–positive areas and α11/PDGFRβ–positive regions. An enrichment of tenascin C was detected at the proximity of α11/PDGFRβ–positive areas (Figure 10C).

Functional assays in the spheroid model were conducted to validate the implication of the PDGFRβ pathway in CAF invasion and CAF-induced tumor cell invasion. Pharmacological inhibition of PDGFRβ and JNK by imatinib and SP600125, respectively (Figure 11, A and C), blocked PDGF-BB–mediated CAF invasion. Importantly, tumor cell invasion in homospheroids was not affected by PDGFRβ or JNK inhibition (Figure 11, B and D). However, tumor cell invasion in heterospheroids with WT CAFs was completely restored to the control baseline by both PDGFRβ and JNK inhibition. Collectively, these findings demonstrate that integrin α11–modulated PDGFRβ/JNK signaling in CAFs is an important pathway to promote cancer cell invasiveness.

Discussion

Tumor cells are not self-supporting entities, and their metastatic abilities are affected by stromal cells, including a heterogeneous population of CAFs. In this study, by using human BC samples and transgenic mice with spontaneous onset of mammary tumors, we identified an integrin α11/PDGFRβ–positive CAF subset displaying tumor-promoting features that is associated with a poor clinical outcome. The link between stromal integrin α11 and PDGFRβ has been established at (a) the transcriptional level in human BC samples by data mining, (b) the histological level in human and murine BC by IHC, (c) the cellular level by immunostaining on CAFs, (d) the molecular level by coimmunoprecipitation assay, and (e) the functional level in in vitro assays. Mechanistically, we uncover a role for integrin α11 in regulating PDGFRβ signaling and its downstream JNK activation, which leads to increased expression of one of its targets, tenascin C, a proinvasive matricellular protein, strongly coexpressed with integrin α11 and PDGFRβ in clinical samples. We provide clear evidence that integrin α11/PDGFRβ molecular crosstalk exploits JNK signaling to endow CAFs with protumorigenic abilities in sustaining the invasiveness of BC cells.

The originality of the present work is to investigate integrin α11, a fibrillar collagen–binding β_1 integrin, mainly expressed by fibroblastic cells. Previous studies already reported that this integrin is expressed by mesenchymal cell types in wound healing and lung cancer (29, 32, 33). Whether or not integrin α11 expression is restricted to a specific CAF subset has not yet been documented. Our study highlights that integrin α11 expression is mostly localized in the stromal compartment of BC and provides evidence for a strong association between integrin α11 and PDGFRβ, both in clinical BC samples and in the preclinical PyMT mouse model. High *PDGFRB* expression has already been correlated with shorter patient survival, and this molecule is proposed as a prognostic marker in many cancer types, including BC (23, 45, 46). Here, Kaplan-Meier analysis revealed that high *ITGA11* expression is correlated with lower overall and metastasis-free survival of patients with BC. Additionally, integrin α11/PDGFRβ colocalization was associated with a poor outcome, including high proliferation rate and histological grade, as well as increased metastasis and mortality. The integrin α11/PDGFRβ coexpression was denser in invasive tumors and mostly confined to the juxta-epithelial fibroblasts. Because of technical limitation related to the lack of anti–integrin α11 antibody suitable on paraffin sections, our IHC study was restricted to frozen BC samples and is worth extending into larger cohorts. Our data are in line with a recent study showing that PDGFRβ$^+$ peritumoral fibroblasts constitute a poor prognosis–associated fibroblast phenotype in DCIS (47). In agreement with the clinical data, *Itga11* deficiency in mice drastically delayed PyMT tumor growth and reduced lung metastasis. Altogether, these findings indicate that integrin α11 exerts a tumor-promoting function and is mostly expressed by a subtype of PDGFRβ$^+$ CAFs. However, we cannot exclude the possibility that integrin α11 displays additional protumoral features in a PDGFRβ-independent manner. Indeed, in both human and murine tumor samples, the α11/PDGFRβ–positive CAF subset represents around 70% of α11$^+$ CAFs, with a remaining population of 30% of α11$^+$PDGFRβ$^-$ CAFs. The moderate increase of the proinvasive activity of α11$^+$ CAFs observed under basal conditions (without PDGF-BB) suggests that this integrin might also be involved in other protumoral effects.

The desmoplastic reaction represents a feature of disease malignancy and patient outcome in human BC (48). Our data mining revealed that *ITGA11* expression strongly correlates with several fibroblastic markers and collagen molecules in human BC, further confirming an association of this integrin with CAFs and the desmoplastic reaction. Moreover, PDGF signaling was also linked to desmoplasia initiation in human BC (49), which additionally supports the synergistic crosstalk between integrin α11 and PDGFRβ. Interestingly, the *ITGA11* upregulation that we initially found in human BC was confirmed in other desmoplastic cancers, including lung, pancreas, colorectal, and gastric cancers. It is worth mentioning that the second fibrillar collagen–binding $\alpha_2\beta_1$ integrin (*ITGA2*) is downregulated in human BC and acts as a metastasis suppressor in a murine model (50). These data suggest opposite effects of the 2 fibrillar collagen–binding integrins ($\alpha_2\beta_1$ and $\alpha_{11}\beta_1$) in BC.

Although PDGFRβ is a well-known marker of pericytes (19), the integrin α11$^+$ cell subset is unlikely to be a pericyte subpopulation, as integrin α11 positivity poorly correlates with αSMA or NG2. Additionally, the absence of an association between α11 and FSP1 positivity suggests that α11$^+$ cells are distinct from normal fibroblasts, as FSP1 was proposed as a marker of quiescent tissue fibroblasts (4) and is poorly expressed in late-stage PyMT tumors used in this study. The slight association between integrin α11 and FAP (22%) might reflect a partial overlap of FAP$^+$, PDGFRβ$^+$, and β_1

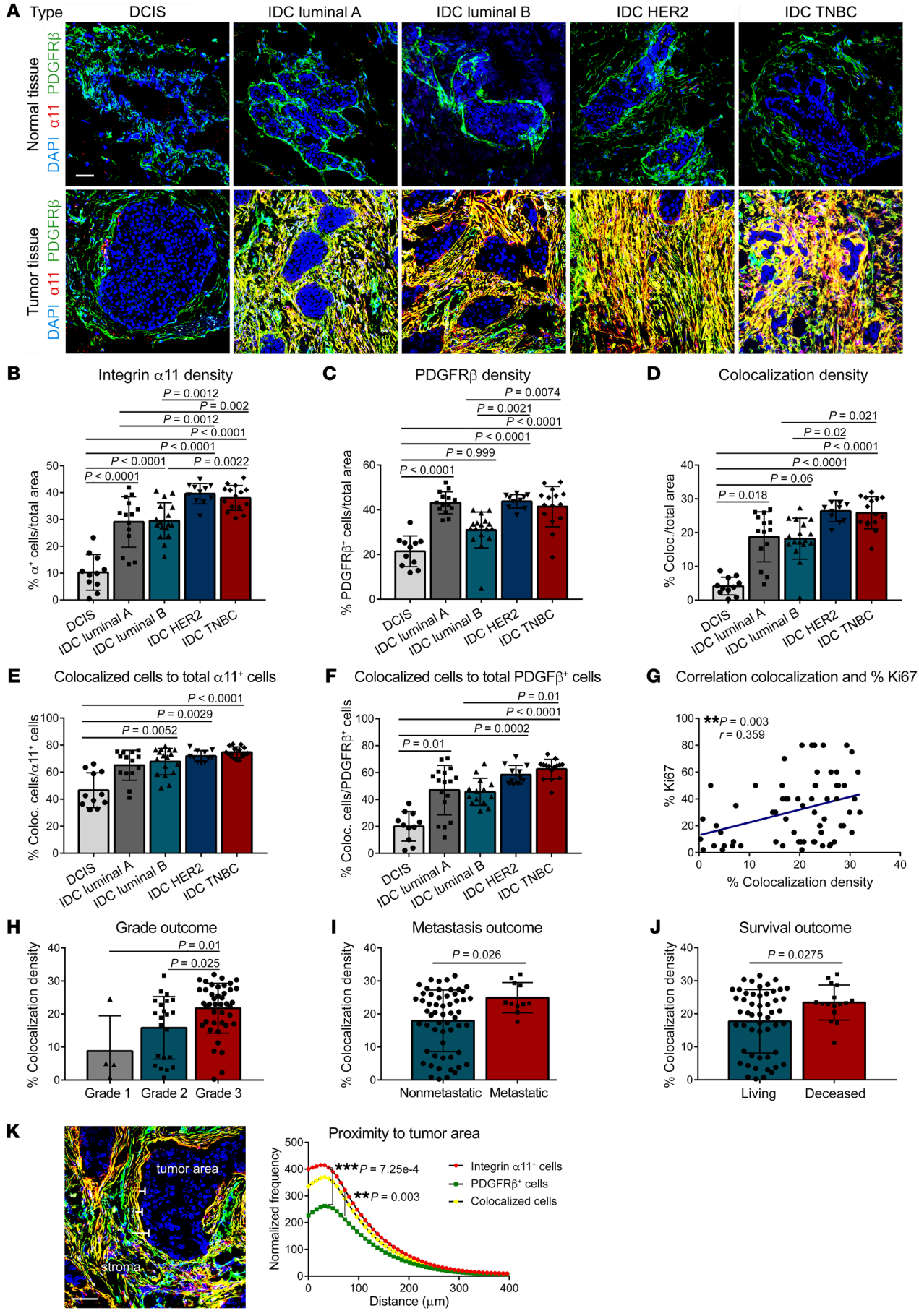
A
Type
DCIS
IDC luminal A
IDC luminal B
IDC HER2
IDC TNBC
Normal tissue
Tumor tissue
DAPI α11 PDGFRβ
B
Integrin α11 density
% α⁺ cells/total area
C
PDGFRβ density
% PDGFRβ⁺ cells/total area
D
Colocalization density
% Coloc./total area
E
Colocalized cells to total α11⁺ cells
% Coloc. cells/α11⁺ cells
F
Colocalized cells to total PDGFβ⁺ cells
% Coloc. cells/PDGFRβ⁺ cells
G
Correlation colocalization and % Ki67
**P = 0.003
r = 0.359
% Ki67
% Colocalization density
H
Grade outcome
% Colocalization density
Grade 1
Grade 2
Grade 3
I
Metastasis outcome
P = 0.026
Nonmetastatic
Metastatic
J
Survival outcome
P = 0.0275
Living
Deceased
K
tumor area
stroma
Proximity to tumor area
Normalized frequency
***P = 7.25e-4
**P = 0.003
Integrin α11⁺ cells
PDGFRβ⁺ cells
Colocalized cells
Distance (μm)

Figure 6. Integrin α11/PDGFRβ density is associated with a poor clinical outcome in BC. (**A**) Representative confocal pictures of immunofluorescence costaining of integrin α11 (red) and PDGFRβ (green) in human breast samples: tumor tissues and normal associated tissues from patients with ductal carcinoma in situ (DCIS) and invasive ductal carcinoma (IDC) of luminal A and B, HER2, or triple-negative (TNBC) breast cancers. Scale bar: 50 μm. Nuclei stained with DAPI (blue). (**B**–**D**) Quantification of density of integrin α11 (**B**), PDGFRβ (**C**), and their colocalization (**D**) on BC samples. Data are presented as percentage of stained area normalized to total tumor area. *n* = 68 patients (*n* = 11 DCIS, *n* = 14 IDC luminal A, *n* = 17 IDC luminal B, *n* = 11 IDC HER2, *n* = 15 IDC TNBC). One-way ANOVA with Dunnett's (**B**) and Kruskal-Wallis with Dunn's multiple-comparisons tests (**C** and **D**). (**E** and **F**) Overall percentage of integrin α11/PDGFRβ–positive cells normalized to total integrin α11$^+$ (**E**) or PDGFRβ$^+$ cells (**F**). Minimum 6 stromal fields per tumor, *n* = 68 patients. Kruskal-Wallis with Dunn's multiple-comparisons test. (**G**) Correlation of integrin α11/PDGFRβ colocalization density from **D** with percentage of Ki67 in human BC. *n* = 68 patients. Pearson correlation analysis. (**H**–**J**) Association of integrin α11/PDGFRβ colocalization density with BC grade (**H**), metastasis (**I**), and survival (**J**) outcomes. *n* = 68 patients. One-way ANOVA with Tukey's multiple-comparisons (**J**) and Mann-Whitney (**H** and **I**) tests. (**K**) Quantification of spatial enrichment of integrin α11 (red), PDGFRβ (green), and colocalization (yellow) areas versus tumor areas in human BC samples. Data are presented as frequency of stained pixels as a function of the distance to tumor areas. *n* = 56 stromal fields. Significance between the distribution curves was determined by Kolmogorov-Smirnov test within the distance range of 0–100 μm.

integrin$^+$ CAF subsets as previously reported (12). Given the multiple putative cellular sources of CAFs, it is possible that host α11$^+$ cells other than resident fibroblasts contribute to tumor growth. This possibility was excluded by transplantation of WT tumors into KO mice leading to tumor growth similar to that in WT mice. This clearly demonstrates that tumor-resident α11$^+$ cells are sufficient for the observed protumoral effects.

A key finding of our study is the ligand-dependent interaction of PDGFRβ with integrin α11 assessed by coimmunoprecipitation and immunofluorescence studies. Importantly, the 2 proteins colocalized at focal adhesions. Along with the classical integrin/ECM signaling, integrin/RTK crosstalk is already documented for several RTKs, including EGFR, IGFR, FGFR, PDGFR, and Met receptors (26, 51). Integrins can promote phosphorylation of RTKs and/or amplify their intracellular signaling. In this context, clustering of cell surface β_1 integrins has been reported to induce PDGFRβ phosphorylation (25). In our system, upon ligand-induced interaction of PDGFRβ with integrin α11, we observed an increase of receptor phosphorylation, suggesting a collaborative signaling between this RTK and integrin α11 (26). When considering downstream mediators of PDGFRβ signaling, we observed a modulation of CRK, SRC, and JNK phosphorylation. CRK and SRC implication in integrin signaling is widely described (52, 53). PDGFRβ is known to bind and phosphorylate CRK adaptor molecules (42). Accordingly, our data demonstrate that α11-PDGFRβ interaction is associated with CRK recruitment assessed by coimmunoprecipitation assay, as well as SRC and JNK activation (see graphical abstract). The absence of integrin α11 does not prevent the formation of CRK/PDGFRβ complex but increases CRK phosphorylation at Y221, the negative regulator site of its activity. Pharmacological inhibition of PDGFRβ by imatinib altered the phosphorylation of CRK, SRC, and JNK. Thus, integrin α11 interaction with PDGFRβ likely favors JNK downstream signaling, rather than classical ERK or AKT pathways. The involvement of additional molecular partners/pathways cannot be excluded.

PDGFRβ or JNK pharmacological inhibition impaired not only CAF invasion but, most importantly, the invasiveness of cancer cells in mixed spheroids. Notably, cancer cells themselves are not sensitive to PDGF-BB stimulation, further highlighting the contribution of integrin α11 in CAF/cancer cell crosstalk. An important finding is that α11$^+$ CAFs issued either from mice or from human patients (4 different subpopulations) were all able to promote tumor cell invasion, independently of intrinsic tumor cell properties. Therefore, α11$^+$ CAFs display a proinvasive activity on tumor cells, and the extent of this effect might be tumor cell–dependent.

The tumor-promoting capacities of CAFs have been widely described as being related to their secretome and their ability to remodel the ECM (4). Our study demonstrates that integrin α11$^+$ CAFs promote cancer cell invasion via cell-cell contact or in a proximal manner. This process could imply the local production of growth factors, migratory modulators, or matrix molecules and/or involve matrix remodeling (54). Integrins have been shown to mediate CAF-induced invasion of cancer cells, by generating tracks within the matrix through the combined action of force- and protease-mediated matrix remodeling (14). Our study provides evidence that the crosstalk between integrin α11 and PDGFRβ and subsequent JNK activation contribute to the acquisition of CAF protumorigenic abilities. The integrin α11/PDGFRβ/JNK molecular axis results in changes in ECM composition with increased deposition of at least one proinvasive matricellular protein (tenascin C). Previous studies have clearly documented that fibroblast-derived tenascin C is a key matricellular protein that promotes tumor cell invasion (14, 55, 56). Notably, its increased expression in tumors is associated with disease progression and metastasis (57). In line with our data, both PDGF and JNK signaling pathways have been reported to regulate tenascin C expression (43, 44). Moreover, our study reveals a strong association between α11/PDGFRβ–positive CAFs and tenascin C expression, particularly in IDC and more aggressive BC molecular subtypes. Although tenascin C regulation contributes to the proinvasive effects exerted by CAFs on tumor cells, we cannot exclude the putative involvement of proteases and other proinvasive ECM molecules in this model.

Collectively, our work sheds a new light on the role played by integrin α11 in BC stroma. This integrin associates mainly with PDGFRβ in a CAF subset displaying tumor-promoting and prometastatic potential. We identify the integrin α11/PDGFRβ/JNK axis as an important mediator of CAF-promoted tumor invasiveness. Pharmacological approaches targeting such a molecular partnership may have strong implications in cancer treatment and prediction of patient response to RTK treatments.

Methods

Generation of Itga11-deficient MMTV-PyMT mouse model. *Itga11*-knockout mice (Itga11^{tm1Dgul}) (35) were backcrossed into an FVB/N background (Harlan Laboratories) for 6 generations, and then crossed with MMTV-PyMT FVB/N transgenic mice expressing polyoma middle T antigen oncogene under mouse mammary tumor virus promoter

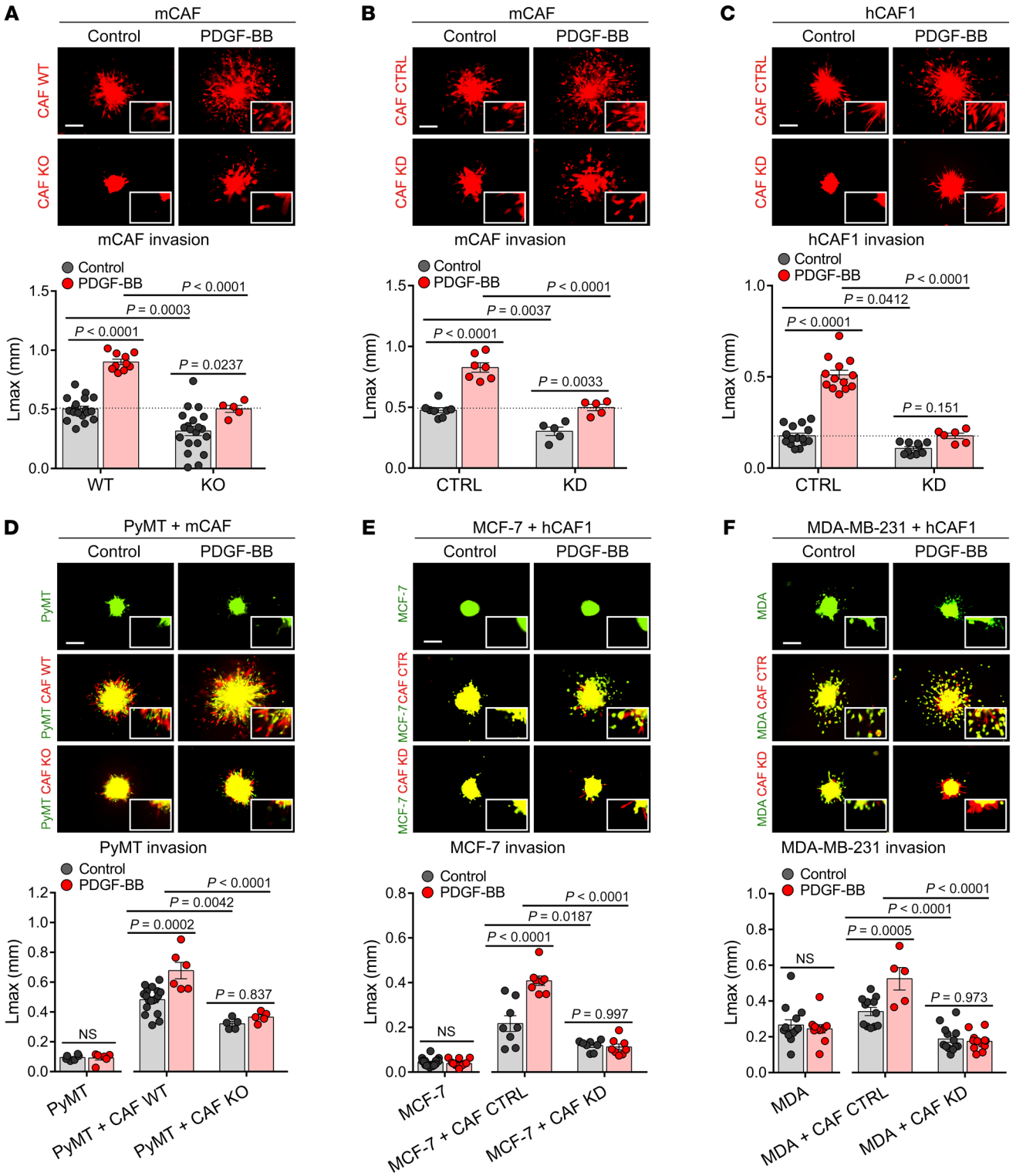

Figure 7. Integrin α11–expressing CAFs promote in vitro tumor cell invasion in response to PDGF-BB. (**A**–**C**) Representative spheroid pictures of red-tracked WT and KO mCAFs (**A**), CTRL and KD mCAFs (**B**), and CTRL and KD hCAF1 (**C**) after 20 hours of invasion in a 3D collagen matrix stimulated with PDGF-BB (10 ng/mL). Scale bars: 200 μm. Zoomed pictures (×2) are in lower right panels. Cell invasion quantification is presented in bottom panels. Data are expressed as maximal distance of invasion from the spheroid border (Lmax). *n* = 5–20 (**A**); *n* = 5–8 (**B**); *n* = 6–15 (**C**). Representative of 3 independent experiments. One-way ANOVA with Tukey's multiple-comparisons test. (**D**–**F**) Representative homo- and hetero-spheroid pictures of green-tracked PyMT tumor cells and red-tracked WT and KO mCAFs (**D**) and green-tracked MCF-7 and MDA-MB-231 tumor cells and red-tracked CTRL and KD hCAF1 (**E** and **F**) after 20 hours of seeding in collagen. Scale bars: 200 μm. Zoomed pictures (×2) in lower right panels. Bottom panels correspond to tumor cell invasion quantification (Lmax). *n* = 5–18 (**D**); *n* = 8–19 (**E**); *n* = 5–13 (**F**). Representative of 3 independent experiments. One-way ANOVA with Tukey's multiple-comparisons test.

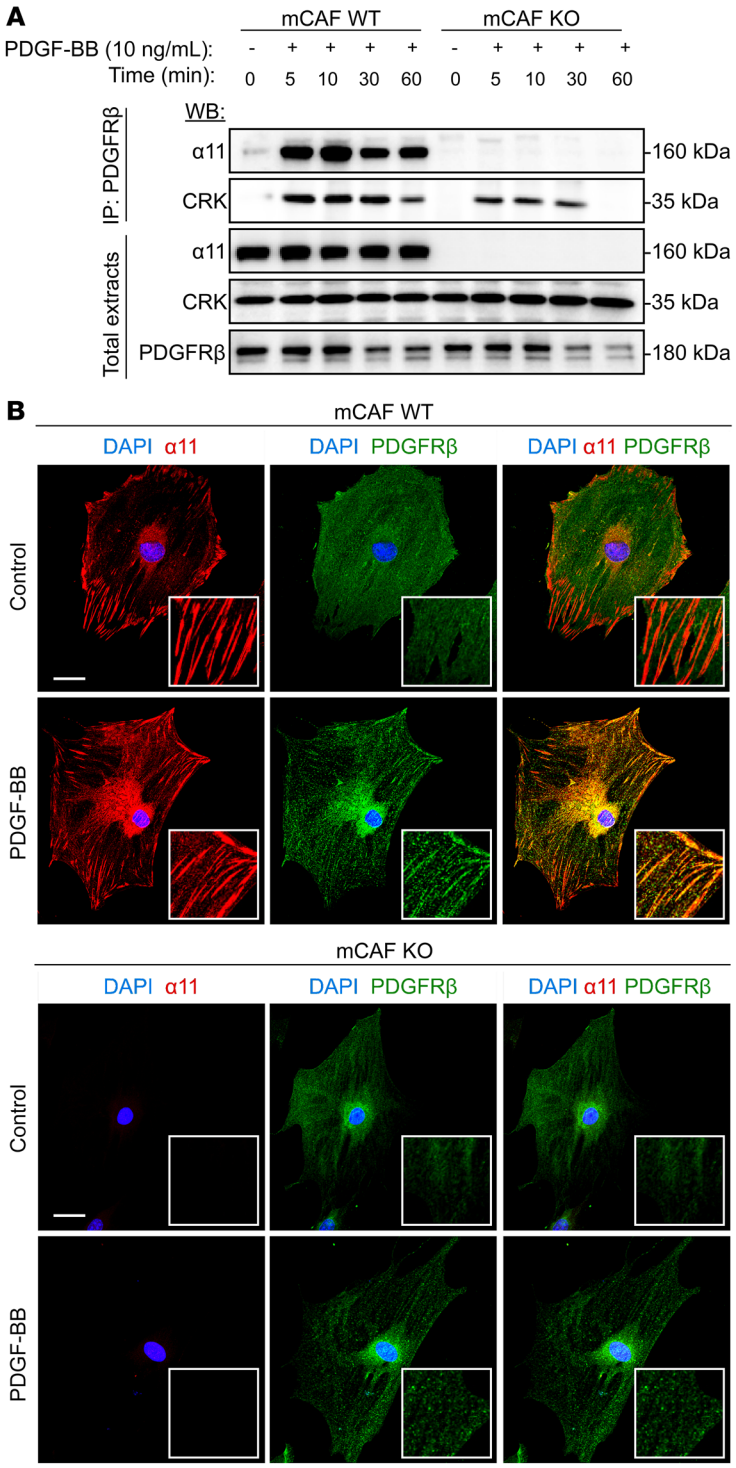

Figure 8. Integrin α11 interacts with PDGFRβ in a ligand-dependent manner. (**A**) Western blot kinetics of PDGFRβ coimmunoprecipitation with integrin α11 and CRK in response to PDGF-BB (10 ng/mL) after 0, 5, 10, 30, and 60 minutes of treatment in WT and KO mCAFs. Total extracts are shown in the corresponding lower panels. (**B**) Confocal immunofluorescence colocalization of integrin α11 (red) and PDGFRβ (green) before (Control) and after treatment with PDGF-BB (10 ng/mL) for 10 minutes in WT and KO mCAFs. Nuclei counterstained with DAPI. Scale bars: 40 μm.

[Tg(MMTV-PyVT)634Mul] for 6 generations (34). All animals were kept within the accredited Mouse Facility and Transgenics GIGA platform of the University of Liège (Liège, Belgium) in specific pathogen–free conditions. Genotyping was performed by PCR of tail genomic DNA as previously described (58). Primer sequences for *Itga11* and PyMT are presented in Supplemental Table 4. Tumor growth was assessed by measurement of the tumor volume (V = length × width^2 × 0.4) twice a week and the tumor mass at sacrifice. Tumor measurement started at week 5 after birth and continued until week 14 for WT and KO groups. For the "KO late" group, *Itga11*-deficient mice were left longer than 14 weeks (maximum until week 18), until they reached the same tumor volume as WT mice at 14 weeks.

For transplantation experiments, matched WT PyMT tumors (11 weeks old, 2-mm fragments) were engrafted into fat pads of FVB/N *Itga11*-WT or -KO mice (aged 10–12 weeks), and tumor volumes were estimated twice a week.

Cell isolation from mouse and human samples. Mouse CAFs (mCAFs) and PyMT tumor cells (PyMT) were isolated from PyMT mice as previously described (59). Late carcinoma tumor samples were surgically removed at week 14. Samples were cut into small pieces and enzymatically digested with a collagenase solution for 45 minutes at 37°C (collagenase type IA, *Clostridium histolyticum*, Sigma-Aldrich, Belgium). After filtration and centrifugation of cell suspension, the pellet was washed, resuspended, and cultured in medium defined below. Cells were plated for 30 minutes to let fibroblasts adhere. The supernatant containing tumor cells was then removed and plated in a separate flask. All PyMT tumor cells were positive for cytokeratin. Primary cultured CAFs were used at early passages (until passage 5 and for no longer than 14 days of culture). CAFs were positive for vimentin and negative for cytokeratin. Human CAFs (hCAFs), isolated in a similar way, were derived from women undergoing a mammectomy with the following tumor characteristics: hCAF1 (99% estrogen receptor–positive, 25% progesterone receptor–positive and HER2-negative), hCAF2 (95% estrogen- and progesterone receptor–positive and HER2-negative), hCAF3 and hCAF4 (triple-negative). Primary cells were isolated by preparation of a single-cell suspension from tumor fragments (1–3 mm^3) followed by culture plate adherent passaging. They were positive for vimentin (100%) and negative for cytokeratin. Primary hCAF2–4 were used until passage 4. The hCAF1 were immortalized after infection with a pBABE retroviral vector expressing the hTERT open reading frame (hTERT hCAF1) and used until passage 8.

Cell culture and siRNA transfection. CAFs, PyMT tumor cells, and human BC cell lines (MCF-7, MDA-MB-231, and SKBr3, obtained from ATCC) were cultured in DMEM (Gibco, Thermo Fisher Scientific) supplemented with 10% FBS, L-glutamine (2 mM), penicillin (100 U/mL), and streptomycin (100 μg/mL) at 37°C and humidified in a 5% CO_2 atmosphere until they reached 90%–100% confluence. Human primary blood (HUVEC) and lymphatic (HMVEC-D) endothelial cells were cultured in EGM2 and EGM2-MV medium (Lonza, Verviers, Belgium), respectively. All cells were mycoplasma-free.

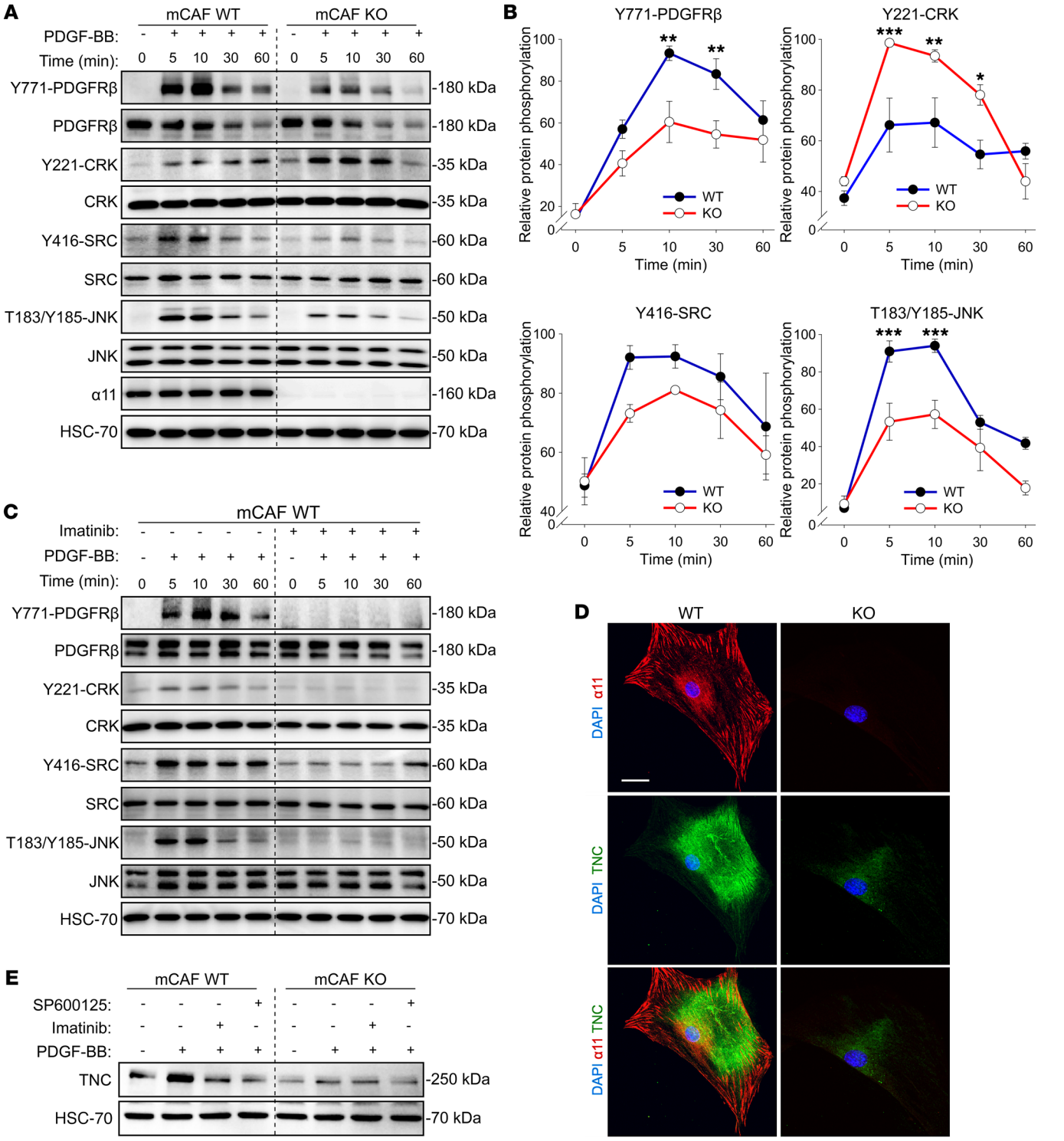

Figure 9. Integrin α11 regulates PDGFRβ downstream activation and promotes tenascin C expression in CAFs. (**A**) Western blot of protein phosphorylation for PDGFRβ (Y771), CRK (Y221), SRC (Y416), and JNK (T183/S185) after 0, 5, 10, 30, and 60 minutes of PDGF-BB (10 ng/mL) stimulation in WT and KO mCAFs. (**B**) Quantified kinetics of PDGFRβ, CRK, SRC, and JNK protein phosphorylation from **A**. Data are presented as normalized ratio between phosphorylated and total proteins. $n = 7$ (Y771-PDGFRβ); $n = 4$ (Y221-CRK); $n = 3$ (Y416-SRC); $n = 4$ (T183/Y185-JNK) of independent experiments. Two-way ANOVA with Holm-Šidák multiple-comparisons test. (**C**) Western blot of protein phosphorylation for PDGFRβ (Y771), CRK (Y221), SRC (Y416), and JNK (T183/S185) after PDGF-BB (10 ng/mL) stimulation in WT mCAFs pretreated or not with imatinib (5 μM) for 1.5 hours. (**D**) Confocal immunofluorescence staining of integrin α11 (red) and tenascin C (TNC) (green) in WT and KO mCAFs. Nuclei stained with DAPI. Scale bar: 40 μm. (**E**) Western blot analysis of tenascin C expression before or after PDGF-BB (10 ng/mL) stimulation in WT and KO mCAFs pretreated or not with imatinib (5 μM) or SP600125 (5 μM) for 20 hours. $^{**}P < 0.01$; $^{***}P < 0.001$.

All human cell lines described above were authenticated before use (Leibniz Institute DSMZ). For *ITGA11*/*Itga11* downregulation, cells at 60%–70% confluence were transfected for 48 hours before experiments with INTERFERin siRNA transfection reagent (Polyplus) and Mouse or Human SMARTpool: ON-TARGETplus *Itga11* siRNA (Dharmacon) (20 nM) in DMEM supplemented with 10% FBS. ON-TARGETplus Non-targeting Control Pool (Dharmacon) was used as negative transfection control. *ITGA11*/*Itga11* downregulation was confirmed after 48–72 hours by Western blot. For Western blot and coimmunoprecipitation experiments, cells were used at 90%–100% confluence after 3 days of seeding. For immunofluorescence confocal detection, low-confluence cells (20%–30%) were used 20 hours after seeding. For PDGF-BB stimulation, high-confluence cells were serum-starved for 2 hours, followed by PDGF-BB stimulation (R&D Systems) (10 ng/mL). For imatinib experiments, high-confluence cells were serum-starved for 2 hours and pretreated with imatinib (LC Laboratories) (5 μM) for 1.5 hours followed by PDGF-BB stimulation.

Bioinformatics analysis. Meta-analysis of global gene expression data in the Oncomine database (60) (Compendia Bioscience, Ann Arbor, Michigan, USA) was performed using primary filters for "breast cancer" and "cancer vs. normal analysis," sample filter for "clinical specimens," and data type filter for "mRNA" data sets (8 data sets representing 2415 patients). Patients of all ages, sexes, disease stages, or treatments were included. Data were acquired in an unbiased manner by compiling of all the Oncomine studies with significantly altered ITGA11 expression at the threshold settings ($P = 0.05$, fold change = 1.5, and gene rank = all) (60). Significant studies in which at least 1 analyzed group was composed of 3 patients or fewer were excluded. All data are reported as $\log_2$ median-centered intensity in the Oncomine database. The data sets were exported from Oncomine and analyzed in GraphPad Prism version 7 software.

The gene expression profiles of GSE8977 (61), GSE9014 (62), GSE14548 (63), GSE33692 (64), GSE41228 (36), and GSE68744 (65) were obtained from the NCBI Gene Expression Omnibus (GEO) database (66), and data were recalculated using the GEO2R analytical tool (67). The $\log_2$-transformed expression values of *ITGA11* were exported from GEO2R and analyzed in GraphPad Prism. Identification of genes whose expression profiles were best correlated with *ITGA11* mRNA levels was performed by interrogation of gene expression data sets contained at cBioPortal and Breast Cancer Gene-Expression Miner (bc-GenExMiner). bc-GenExMiner contains 36 data sets including 5861 BC patients (68). cBioPortal was used to explore the TCGA breast (69) and METABRIC (70) cohorts. For each of these 3 patient cohorts (referred to as TCGA, METABRIC, and GenExMiner), genes with Pearson's correlation coefficients greater than 0.5 were selected and classified as being *ITGA11*-coexpressed genes. The intersections of coexpressed genes from the 3 cohorts were analyzed using the Venny 2.1 online tool. Kaplan-Meier curves were generated with the Kaplan-Meier plotter website (http://kmplot.com/analysis/), using a database of public microarray data sets (71). Automatic cutoff scores were selected during queries; overall survival (OS) and distant metastasis–free survival (DMFS) were selected. Log-rank *P* values were computed as previously described (71). Integrative coexpression network was analyzed in the TCSBN database as previously described (38).

Histological analysis. Mouse tumor and lung samples were formalin-fixed (4%) and paraffin-embedded. Sections of 6 μm thickness were counterstained with H&E and mounted with Eukitt medium for light microscope observation. For desmoplasia analysis, a Van Gieson staining was performed by incubation of slides with Weigert's iron hematoxylin solution followed by Van Gieson staining (Sigma-Aldrich, Belgium). Slides were scanned using the NanoZoomer 2.0-HT system (Hamamatsu, Belgium), and automatic quantification was performed with the image analysis toolbox of MATLAB 8.3 software (MathWorks Inc.). Desmoplasia was expressed as collagen density normalized to total tumor area. For metastasis quantification, 6 lung sections, each taken at a distance of between 6 μm and 10 μm, were analyzed for each mouse. Metastatic index was calculated by division of the tumor lung area by the total lung area.

Immunofluorescence studies. For colocalization studies on mouse samples, cryosections embedded in OCT (6 μm thickness) were fixed in acetone at –20°C for 10 minutes, followed by rehydration and blocking in Protein Block, Serum-Free Solution (Dako, Agilent) for 10 minutes. Primary and secondary antibodies (references and dilutions in Supplemental Table 5) were incubated sequentially in Antibody Diluent with Background Reducing Components (Dako, Agilent). Slides were mounted in DAPI Fluoromount-G (SouthernBiotech) and analyzed within 48 hours after staining. For integrin α11 and PDGFRβ colocalization on human samples, cryosections of human carcinoma and the associated normal breast tissues were analyzed for the following groups: ductal carcinoma in situ (DCIS) and invasive ductal carcinomas (IDCs) of luminal A and B, HER2, and TNBC cancers (68 patients). For detection of integrin α11 on human samples, the anti-human Mab203E1H5 antibody was produced (72) (antibody deposited under Patent Application EP18155716, European Patent Office). All samples were analyzed by confocal Olympus Fluoview 1000 microscopy in Kalman filter mode with a ×20-magnification objective. For image analysis and quantification, protein expression hotspots were identified within tumor sections (at least 6 stromal fields per sample), and integrin α11, PDGFRβ, and colocalization densities were quantified by specifically designed algorithm in MATLAB 8.3 software. The proximity analysis was performed by identification of the Euclidean distance from each pixel belonging to integrin $\alpha11^+$, $PDGFR\beta^+$, and colocalized positive areas to tumor nodules. Pictures lacking defined tumor areas were excluded. For triple colocalization, the proximity of tenascin C to the colocalized integrin α11/PDGFRβ areas was calculated as described above. For immunofluorescence studies on CAFs, low-confluence cells (20%–30%) were fixed in methanol/acetone mixture (80/20) at –20°C for 10 minutes, followed by rehydration and blocking in Innovex Background Buster (Innovex Biosciences) for 10 minutes. Cells were incubated with primary and secondary antibodies as described above. Samples were analyzed by confocal Olympus Fluoview 1000 microscopy in Kalman filter mode with a ×60-magnification oil immersion objective.

Collagen contraction assay. For each replicate, 2×10^5 cells were suspended in 700 μL of native collagen solution (2 mg/mL) buffered at pH = 7.5 (rat tail Collagen I, Corning) and seeded in a 12-well plate pretreated with 2% BSA solution. After collagen polymerization at 37°C, gels were detached carefully from the well border, and medium supplemented with 5% FBS was added. Collagen lattice contraction was monitored for 96 hours by taking of pictures daily with an LAS-4000 image analyzer (Fujifilm, Belgium). Gel area was measured by ImageJ (NIH) software, and the percentage of gel reduction was calculated by subtraction of the gel area for each day from the gel area at time 0 hours.

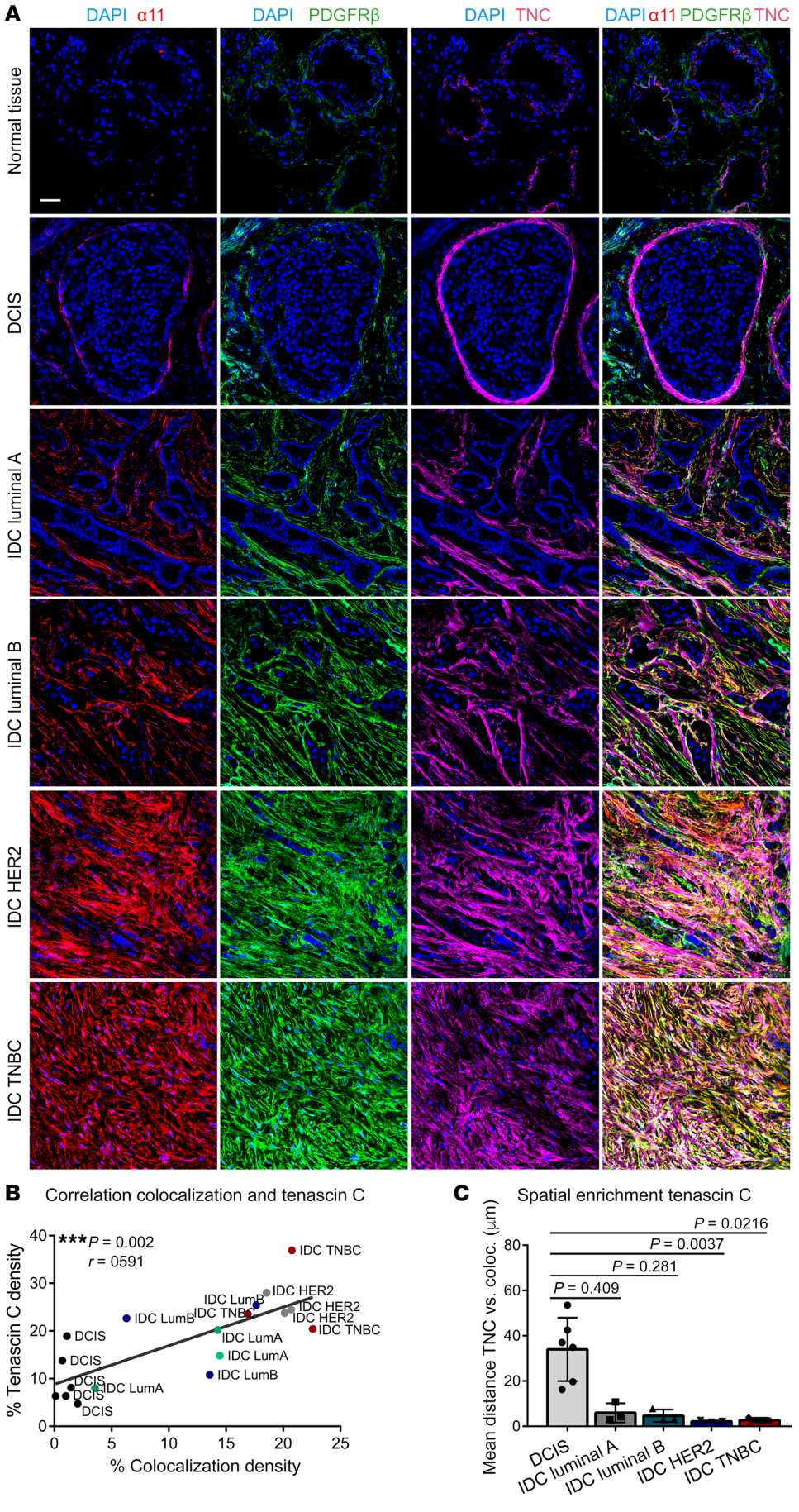

Figure 10. Integrin α11/PDGFRβ density is associated with tenascin C enrichment in human BC. (**A**) Representative immunofluorescence pictures of integrin α11 (red), PDGFRβ (green), and tenascin C (TNC) (pink) costaining in human breast samples: normal associated breast tissue, ductal carcinoma in situ (DCIS), and invasive ductal carcinomas (IDC) from luminal A and B, HER2, or TNBC patients. Scale bar: 50 μm. Nuclei stained with DAPI. (**B**) Correlation of integrin α11/PDGFRβ colocalization density with TNC expression on human BC samples from **A**. Data are presented as percentage of density (stained area/total tumor area). *n* = 18 patients (*n* = 6 DCIS, *n* = 3 IDC luminal A, *n* = 3 IDC luminal B, *n* = 3 IDC HER2, *n* = 3 IDC TNBC). Pearson correlation analysis. (**C**) Spatial enrichment of TNC versus integrin α11/PDGFRβ colocalized areas in BC samples from **A** and **B**. Data are presented as mean of the Euclidean distance of TNC to colocalized areas. *n* = 18 patients. Kruskal-Wallis with Dunn's multiple-comparisons test.

Spheroid invasion assay. For fluorescence cell tracking, CAFs and tumor cells were incubated for 30 minutes in serum-free medium with CellTracker Green CMFDA or Orange CMRA (Invitrogen, Thermo Fisher Scientific). Spheroids were prepared by seeding of 500 CAFs or 1000 tumor cells (homospheroids) or a mixture of both (heterospheroids) in 200 μL of DMEM supplemented with 10% FBS and containing 20% of carboxymethylcellulose 4000 cP (Sigma-Aldrich). Cells were seeded in round-bottom nonadherent 96-well plates (CELLSTAR, Greiner Bio-One) for 24 hours for spheroid formation. The following day, single spheroids were collected from wells, centrifuged, and suspended in 500 μL/well of native collagen solution (2 mg/mL; rat tail Collagen I, Corning) at pH 7.5 and seeded in collagen-precoated 12-well plates (15 spheroids per well; 2 wells per condition). After collagen polymerization, 500 μL of DMEM supplemented with 2% FBS was carefully added. For PDGF-BB stimulation, spheroids were treated with recombinant human PDGF-BB (10 ng/mL; R&D Systems). In some assays, imatinib (LC Laboratories) and SP600125 (Sigma-Aldrich) were added (5 μM). Spheroids were analyzed after 20 hours of culture, and image acquisition was performed by epifluorescence Nikon Eclipse Ti microscope (×10-magnification objective). Image analysis was performed as previously described (73). Cell invasion was automatically quantified by specifically designed algorithm in MATLAB 8.3 software. Data were expressed as the maximal distance of cell invasion from the spheroid border.

RNA extraction and quantitative reverse transcriptase PCR analysis. Total tumor RNA was extracted using the RNeasy Mini Kit (Qiagen GmbH). RNA was quantified and purity checked with the ND-1000 NanoDrop spectrophotometer (NanoDrop Technologies). Quantitative reverse transcriptase PCR was performed on reverse-transcribed RNA (First Strand cDNA Synthesis kit, Roche) with LightCycler480 Probes Master kit (Roche) and the Universal Probe Library system (Roche) using specific primers (Eurogentec). Data were normalized to mouse TBP. Primer nucleotide sequences are indicated in Supplemental Table 4.

Western blot and coimmunoprecipitation analysis. For protein extraction, frozen tumor samples or fresh cells were suspended in Lysis Buffer (Cell Signaling Technology) supplemented with Complete protease and PhoStop phosphatase inhibitor cocktails (Roche). Tumor samples were homogenized with the MagnaLyser system (Roche), while cell samples were scraped on ice. After centrifugation at 14,000 *g* for 10 minutes at 4°C, proteins were quantified with the DC protein assay kit (Bio-Rad Laboratories). Tumor (100 μg) or cell extracts (20 μg) were separated by SDS-PAGE under reducing conditions. PVDF membranes (PerkinElmer Life Sciences) were incubated for 1 hour in 5% nonfat dry milk or BSA PBS solution, followed by overnight incubation with primary antibodies. Antibodies and dilutions are indicated in Supplemental Table 5. Immunocomplexes were detected with an ECL-Plus enhanced chemiluminescence system and visualized with an image analyzer (LAS-4000; Fujifilm, Belgium). Band densities were quantified with Quantity-One software (Bio-Rad Laboratories). For loading control, membranes were incubated with HSC-70 antibody. For phosphorylation experiments, membranes were stripped in Restore Western Blot Stripping Buffer (Thermo Fisher Scientific), reblocked, and reincubated with antibodies for total protein detection. For coimmunoprecipitation analysis, 700 μg of protein extracts were immunoprecipitated overnight with PDGFRβ antibody (clone 2B3, Cell Signaling Technology) according to the manufacturer's instructions. Protein complexes were resuspended in Dynabeads Protein G solution (50 μL; Thermo Fisher Scientific) and incubated for 8 hours at 4°C. Protein-bead complexes were collected from a magnet system, washed, and resuspended in Lysis Buffer and heated for 5 minutes at 95°C. Samples were next analyzed by Western blot. Total protein extracts, CAF KO, IgG, and input samples were used as immunoprecipitation controls.

Statistics. Unless otherwise stated, statistical analysis was performed with SigmaPlot and GraphPad Prism software, and results are expressed as mean ± SEM. For 2-group comparison, 2-tailed unpaired *t* test or Mann-Whitney test was performed. For multiple-group comparison, 1-way ANOVA or Kruskal-Wallis tests were performed with the multiple-comparison post hoc correction as indicated. Equality-of-variance test between groups and Shapiro-Wilk normality test were performed, and statistical tests were chosen accordingly. Graphs show exact *P* values or asterisks *P* less than 0.05 was considered significant.

Study approval. All animal experiments were conducted at the GIGA Animal Facility of the University of Liège (ULiège; Belgium) in accordance with the Federation of European Laboratory Animal Science Associations and the local ethical committee at ULiège. Cryosections of human BC samples and related normal associated tissues (*n* = 68 including 11 DCIS, 14 IDC luminal A, 17 IDC luminal B, 11 IDC HER2, and 15 IDC TNBC) were provided by the Biobank of the University Hospital of Liège for a retrospective study in accordance with current legislation and recommendations of the Ethical Committee of the University Hospital of Liège.

Author contributions

IP established *Itga11*$^{-/-}$ MMTV-PyMT mice, designed, performed, and analyzed all experiments, and wrote the manuscript. EM conducted in silico data analysis and wrote the manuscript. SB and TL performed all computerized quantification. AC contributed to *Itga11* PyMT mouse breeding. HYHS and LS contributed to immunostaining. JVD and ODW provided hCAFs and contributed to data interpretation. NES, CP, and DC participated in experimental design and data interpretation. RH and TP established and provided the *Itga11*$^{-/-}$ FVB/N mice. DG contributed to data interpretation and provided ITGA11 tools. AN supervised, funded, and designed the project, interpreted the data, and wrote the manuscript.

Acknowledgments

We thank all laboratory members for useful technical advice, and all members of Marie Curie CAFFEIN Innovative Training Network (ITN) for valuable scientific discussions. We thank GIGA Imaging and Animal Facility platforms of ULiège for technical support and mouse housing. We thank the Biobank of ULiège for providing BC samples. This project was part of the CAFFEIN FP7 ITN consortium and received funding from the People Program (Marie Curie Actions) of the European Union's Seventh Framework Program FP7/2007-2013/ under Research Executive Agency grant agreement 316610. The opinions presented in this article reflect only the authors' views, and the European Union is not liable for any use that may be made of the information contained herein. This work was supported by grants from the Fonds de la Recherche Scientifique (FRS-FNRS,

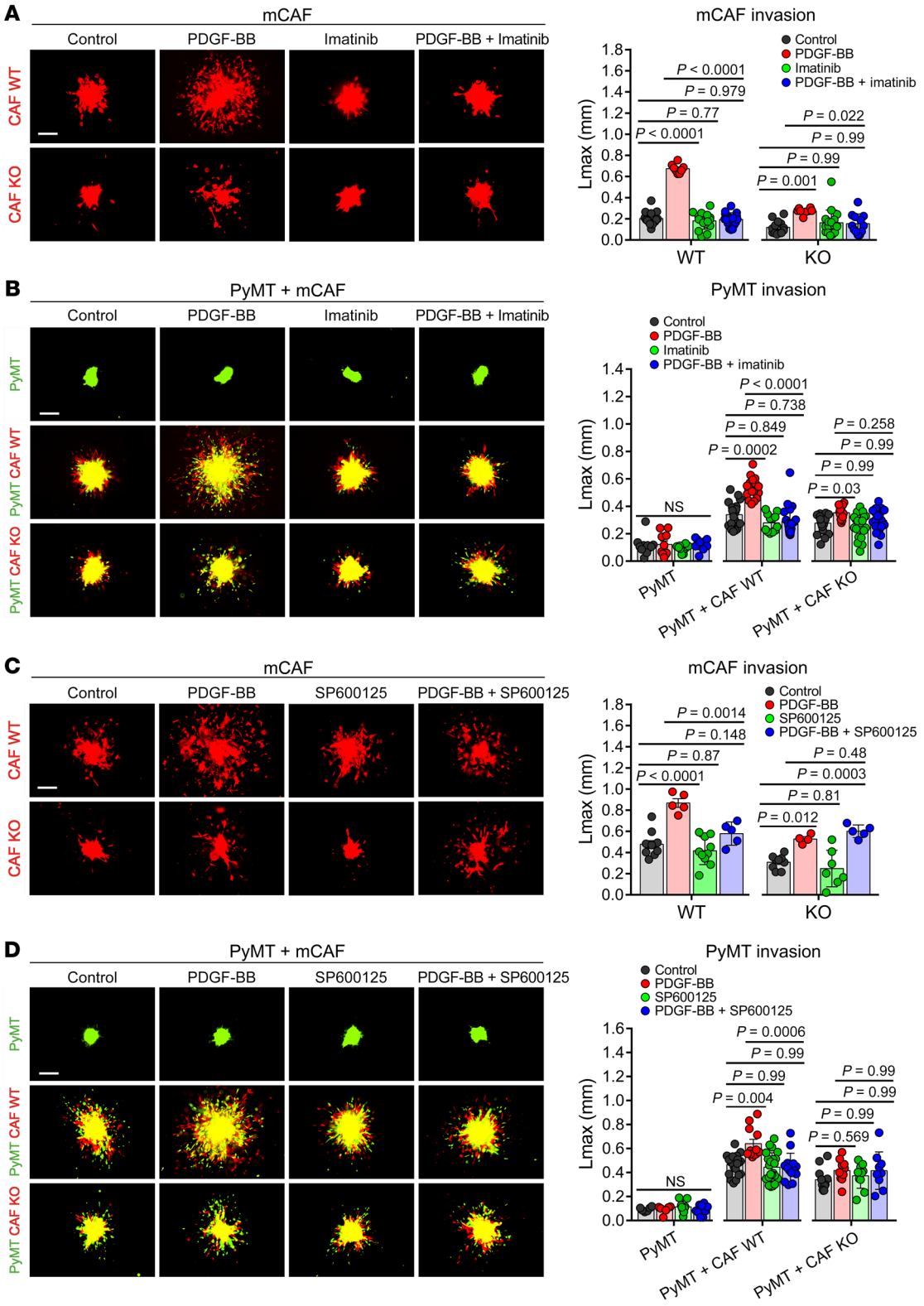

Figure 11. Pharmacological inhibition of PDGFRβ or JNK reverses PDGF-BB–induced invasiveness of integrin α11–WT CAFs and of cancer cells in heterospheroids. (**A** and **C**) Representative homospheroid pictures of red-tracked WT and KO mCAFs after 20 hours of invasion in collagen in response to PDGF-BB (10 ng/mL) and upon treatment with 5 μM of imatinib (PDGFRβ inhibition) (**A**) or SP600125 (JNK inhibition) (**C**). Scale bars: 200 μm. Quantification of cell invasion is presented in the corresponding graphs. Data are expressed as maximal distance of invasion from the spheroid border (Lmax). *n* = 8–17 (**A**); *n* = 5–11 (**C**). Kruskal-Wallis with Dunn's multiple-comparisons (**A**) and 1-way ANOVA with Tukey's multiple-comparisons (**C**) tests. (**B** and **D**) Representative homo- and heterospheroid pictures of green-tracked PyMT tumor cells and red-tracked WT and KO mCAFs after 20 hours of invasion in response to PDGF-BB (10 ng/mL) and upon treatment with 5 μM of imatinib (**B**) or SP600125 (**D**). Scale bars: 200 μm. Quantification of tumor cell invasion (Lmax) is presented in the corresponding graphs. *n* = 12–21 (**B**); *n* = 9–22 (**D**). Kruskal-Wallis with Dunn's multiple-comparisons test.

Belgium), the Fondation contre le Cancer (Foundation of Public Interest, Belgium), the Fonds Spéciaux de la Recherche (University of Liège), the Fondation Hospital-Universitaire Léon Frédéricq (University of Liège), the Research Council of Norway through its Centres of Excellence funding scheme (project 223250), the Academy of Finland Research Council for Health (grant 308867), and the Sigrid Jusélius Foundation, IUAP Belspo. AC and TL are supported by FNRS-Televie fellowships. EM is a Research Associate from FNRS (Belgium).

Address correspondence to: Agnès Noel, GIGA-Cancer, Laboratoire de Biologie des Tumeurs et du Développement, Avenue Hippocrate, 13, Tour de Pathologie B23/+4, Sart-Tilman, 4000 Liège, Belgium. Phone: 04.366.25.68; Email: agnes.noel@uliege.be.

1. Pan H, et al. 20-Year risks of breast-cancer recurrence after stopping endocrine therapy at 5 years. *N Engl J Med*. 2017;377(19):1836–1846.
2. Hanahan D, Coussens LM. Accessories to the crime: functions of cells recruited to the tumor microenvironment. *Cancer Cell*. 2012;21(3):309–322.
3. Orimo A, Weinberg RA. Heterogeneity of stromal fibroblasts in tumors. *Cancer Biol Ther*. 2007;6(4):618–619.
4. Kalluri R. The biology and function of fibroblasts in cancer. *Nat Rev Cancer*. 2016;16(9):582–598.
5. LeBleu VS, Kalluri R. A peek into cancer-associated fibroblasts: origins, functions and translational impact. *Dis Model Mech*. 2018;11(4):dmm029447.
6. Sun KH, Chang Y, Reed NI, Sheppard D. α-Smooth muscle actin is an inconsistent marker of fibroblasts responsible for force-dependent TGFβ activation or collagen production across multiple models of organ fibrosis. *Am J Physiol Lung Cell Mol Physiol*. 2016;310(9):L824–L836.
7. Öhlund D, Elyada E, Tuveson D. Fibroblast heterogeneity in the cancer wound. *J Exp Med*. 2014;211(8):1503–1523.
8. Gascard P, Tlsty TD. Carcinoma-associated fibroblasts: orchestrating the composition of malignancy. *Genes Dev*. 2016;30(9):1002–1019.
9. Hanahan D, Weinberg RA. Hallmarks of cancer: the next generation. *Cell*. 2011;144(5):646–674.
10. Orimo A, et al. Stromal fibroblasts present in invasive human breast carcinomas promote tumor growth and angiogenesis through elevated SDF-1/CXCL12 secretion. *Cell*. 2005;121(3):335–348.
11. Erez N, Truitt M, Olson P, Arron ST, Hanahan D. Cancer-associated fibroblasts are activated in incipient neoplasia to orchestrate tumor-promoting inflammation in an NF-kappaB-dependent manner. *Cancer Cell*. 2010;17(2):135–147.
12. Costa A, et al. Fibroblast heterogeneity and immunosuppressive environment in human breast cancer. *Cancer Cell*. 2018;33(3):463–479.
13. Zhang D, et al. Metabolic reprogramming of cancer-associated fibroblasts by IDH3α downregulation. *Cell Rep*. 2015;10(8):1335–1348.
14. Gaggioli C, et al. Fibroblast-led collective invasion of carcinoma cells with differing roles for RhoGTPases in leading and following cells. *Nat Cell Biol*. 2007;9(12):1392–1400.
15. De Vlieghere E, Verset L, Demetter P, Bracke M, De Wever O. Cancer-associated fibroblasts as target and tool in cancer therapeutics and diagnostics. *Virchows Arch*. 2015;467(4):367–382.
16. Özdemir BC, et al. Depletion of carcinoma-associated fibroblasts and fibrosis induces immunosuppression and accelerates pancreas cancer with reduced survival. *Cancer Cell*. 2014;25(6):719–734.
17. Rhim AD, et al. Stromal elements act to restrain, rather than support, pancreatic ductal adenocarcinoma. *Cancer Cell*. 2014;25(6):735–747.
18. Roswall P, et al. Microenvironmental control of breast cancer subtype elicited through paracrine platelet-derived growth factor-CC signaling. *Nat Med*. 2018;24(4):463–473.
19. Östman A. PDGF receptors in tumor stroma: biological effects and associations with prognosis and response to treatment. *Adv Drug Deliv Rev*. 2017;121:117–123.
20. Frings O, et al. Prognostic significance in breast cancer of a gene signature capturing stromal PDGF signaling. *Am J Pathol*. 2013;182(6):2037–2047.
21. Ostman A, Heldin CH. PDGF receptors as targets in tumor treatment. *Adv Cancer Res*. 2007;97:247–274.
22. Paulsson J, et al. High expression of stromal PDGFRβ is associated with reduced benefit of tamoxifen in breast cancer. *J Pathol Clin Res*. 2017;3(1):38–43.
23. Paulsson J, et al. Prognostic significance of stromal platelet-derived growth factor beta-receptor expression in human breast cancer. *Am J Pathol*. 2009;175(1):334–341.
24. Yamada KM, Even-Ram S. Integrin regulation of growth factor receptors. *Nat Cell Biol*. 2002;4(4):E75–E76.
25. Sundberg C, Rubin K. Stimulation of beta1 integrins on fibroblasts induces PDGF independent tyrosine phosphorylation of PDGF beta-receptors. *J Cell Biol*. 1996;132(4):741–752.
26. Ivaska J, Heino J. Cooperation between integrins and growth factor receptors in signaling and endocytosis. *Annu Rev Cell Dev Biol*. 2011;27:291–320.
27. Zeltz C, Lu N, Gullberg D. Integrin α11β1: a major collagen receptor on fibroblastic cells. *Adv Exp Med Biol*. 2014;819:73–83.
28. Barczyk MM, Lu N, Popova SN, Bolstad AI, Gullberg D. α11β1 integrin-mediated MMP-13-dependent collagen lattice contraction by fibroblasts: evidence for integrin-coordinated collagen proteolysis. *J Cell Physiol*. 2013;228(5):1108–1119.
29. Zeltz C, Gullberg D. The integrin-collagen connection—a glue for tissue repair? *J Cell Sci*. 2016;129(4):653–664.
30. Carracedo S, Lu N, Popova SN, Jonsson R, Eckes B, Gullberg D. The fibroblast integrin alpha11beta1 is induced in a mechanosensitive manner involving activin A and regulates myofibroblast differentiation. *J Biol Chem*. 2010;285(14):10434–10445.
31. Schulz JN, et al. Reduced granulation tissue and wound strength in the absence of α11β1 integrin. *J Invest Dermatol*. 2015;135(5):1435–1444.
32. Zhu CQ, et al. Integrin alpha 11 regulates IGF2 expression in fibroblasts to enhance tumorigenicity of human non-small-cell lung cancer cells. *Proc Natl Acad Sci U S A*. 2007;104(28):11754–11759.
33. Navab R, et al. Integrin α11β1 regulates cancer stromal stiffness and promotes tumorigenicity and metastasis in non-small cell lung cancer. *Oncogene*. 2016;35(15):1899–1908.
34. Guy CT, Cardiff RD, Muller WJ. Induction of mammary tumors by expression of polyomavirus middle T oncogene: a transgenic mouse model for metastatic disease. *Mol Cell Biol*. 1992;12(3):954–961.
35. Popova SN, et al. Alpha11 beta1 integrin-dependent regulation of periodontal ligament function in the erupting mouse incisor. *Mol Cell Biol*. 2007;27(12):4306–4316.
36. Lee S, et al. Differentially expressed genes regulating the progression of ductal carcinoma in situ to invasive breast cancer. *Cancer Res*. 2012;72(17):4574–4586.
37. Croft D, et al. Reactome: a database of reactions, pathways and biological processes. *Nucleic Acids Res*. 2011;39(Database issue):D691–D697.
38. Lee S, et al. TCSBN: a database of tissue and cancer specific biological networks. *Nucleic Acids Res*. 2018;46(D1):D595–D600.
39. Sorokin A, Reed E, Nnkemere N, Dulin NO, Schlessinger J. Crk protein binds to PDGF receptor and insulin receptor substrate-1 with different modulating effects on PDGF- and insulin-dependent signaling pathways. *Oncogene*. 1998;16(19):2425–2434.
40. Bell ES, Park M. Models of crk adaptor proteins in cancer. *Genes Cancer*. 2012;3(5-6):341–352.
41. Antoku S, Mayer BJ. Distinct roles for Crk adaptor isoforms in actin reorganization induced by extracellular signals. *J Cell Sci*. 2009;122(pt 22):4228–4238.
42. Matsumoto T, et al. Differential interaction of CrkII adaptor protein with platelet-derived growth factor alpha- and beta-receptors is determined by its internal tyrosine phosphorylation. *Biochem Biophys Res Commun*. 2000;270(1):28–33.
43. Islam MS, et al. PDGF and TGF-β promote tenascin-C expression in subepithelial myofibroblasts and contribute to intestinal mucosal protection in mice. *Br J Pharmacol*. 2014;171(2):375–388.
44. Insua-Rodríguez J, et al. Stress signaling in breast cancer cells induces matrix components that promote chemoresistant metastasis. *EMBO Mol Med*. 2018;10(10):e9003.
45. Weissmueller S, et al. Mutant p53 drives pancreatic cancer metastasis through cell-autonomous PDGF receptor β signaling. *Cell*. 2014;157(2):382–394.
46. Frödin M, et al. Perivascular PDGFR-β is an independent marker for prognosis in renal cell carcinoma. *Br J Cancer*. 2017;116(2):195–201.
47. Strell C, et al. Impact of epithelial-stromal interactions on peritumoral fibroblasts in ductal carcinoma in situ. *J Natl Cancer Inst*. 2019(9):djy234.

48. Nazari SS, Mukherjee P. An overview of mammographic density and its association with breast cancer. *Breast Cancer*. 2018;25(3):259–267.
49. Shao ZM, Nguyen M, Barsky SH. Human breast carcinoma desmoplasia is PDGF initiated. *Oncogene*. 2000;19(38):4337–4345.
50. Ramirez NE, et al. The $\alpha_2\beta_1$ integrin is a metastasis suppressor in mouse models and human cancer. *J Clin Invest*. 2011;121(1):226–237.
51. Hamidi H, Ivaska J. Every step of the way: integrins in cancer progression and metastasis. *Nat Rev Cancer*. 2018;18(9):533–548.
52. Giancotti FG, Ruoslahti E. Integrin signaling. *Science*. 1999;285(5430):1028–1032.
53. Seguin L, Desgrosellier JS, Weis SM, Cheresh DA. Integrins and cancer: regulators of cancer stemness, metastasis, and drug resistance. *Trends Cell Biol*. 2015;25(4):234–240.
54. Desgrosellier JS, Cheresh DA. Integrins in cancer: biological implications and therapeutic opportunities. *Nat Rev Cancer*. 2010;10(1):9–22.
55. De Wever O, et al. Tenascin-C and SF/HGF produced by myofibroblasts in vitro provide convergent pro-invasive signals to human colon cancer cells through RhoA and Rac. *FASEB J*. 2004;18(9):1016–1018.
56. Xia S, Lal B, Tung B, Wang S, Goodwin CR, Laterra J. Tumor microenvironment tenascin-C promotes glioblastoma invasion and negatively regulates tumor proliferation. *Neuro-oncology*. 2016;18(4):507–517.
57. Lowy CM, Oskarsson T. Tenascin C in metastasis: a view from the invasive front. *Cell Adh Migr*. 2015;9(1-2):112–124.
58. Popova SN, Rodriguez-Sánchez B, Lidén A, Betsholtz C, Van Den Bos T, Gullberg D. The mesenchymal alpha11beta1 integrin attenuates PDGF-BB-stimulated chemotaxis of embryonic fibroblasts on collagens. *Dev Biol*. 2004;270(2):427–442.
59. Calvo F, et al. Mechanotransduction and YAP-dependent matrix remodelling is required for the generation and maintenance of cancer-associated fibroblasts. *Nat Cell Biol*. 2013;15(6):637–646.
60. Rhodes DR, et al. ONCOMINE: a cancer microarray database and integrated data-mining platform. *Neoplasia*. 2004;6(1):1–6.
61. Karnoub AE, et al. Mesenchymal stem cells within tumour stroma promote breast cancer metastasis. *Nature*. 2007;449(7162):557–563.
62. Finak G, et al. Stromal gene expression predicts clinical outcome in breast cancer. *Nat Med*. 2008;14(5):518–527.
63. Ma XJ, Dahiya S, Richardson E, Erlander M, Sgroi DC. Gene expression profiling of the tumor microenvironment during breast cancer progression. *Breast Cancer Res*. 2009;11(1):R7.
64. Knudsen ES, Ertel A, Davicioni E, Kline J, Schwartz GF, Witkiewicz AK. Progression of ductal carcinoma in situ to invasive breast cancer is associated with gene expression programs of EMT and myoepithelia. *Breast Cancer Res Treat*. 2012;133(3):1009–1024.
65. Oh EY, et al. Extensive rewiring of epithelial-stromal co-expression networks in breast cancer. *Genome Biol*. 2015;16:128.
66. Barrett T, et al. NCBI GEO: archive for functional genomics data sets—update. *Nucleic Acids Res*. 2013;41(Database issue):D991–D995.
67. Davis S, Meltzer PS. GEOquery: a bridge between the Gene Expression Omnibus (GEO) and BioConductor. *Bioinformatics*. 2007;23(14):1846–1847.
68. Jézéquel P, et al. bc-GenExMiner: an easy-to-use online platform for gene prognostic analyses in breast cancer. *Breast Cancer Res Treat*. 2012;131(3):765–775.
69. Ciriello G, et al. Comprehensive molecular portraits of invasive lobular breast cancer. *Cell*. 2015;163(2):506–519.
70. Pereira B, et al. The somatic mutation profiles of 2,433 breast cancers refines their genomic and transcriptomic landscapes. *Nat Commun*. 2016;7:11479.
71. Győrffy B, et al. An online survival analysis tool to rapidly assess the effect of 22,277 genes on breast cancer prognosis using microarray data of 1,809 patients. *Breast Cancer Res Treat*. 2010;123(3):725–731.
72. Zeltz C, et al. α11β1 integrin is induced in a subset of cancer-associated fibroblasts in desmoplastic tumor stroma and mediates in vitro cell migration. *Cancers*. 2019;11(6):E765.
73. Blacher S, et al. Cell invasion in the spheroid sprouting assay: a spatial organisation analysis adaptable to cell behaviour. *PLoS One*. 2014;9(5):e97019.
74. Curtis C, et al. The genomic and transciptomic architecture of 2,000 breast tumours reveals novel subgroups. *Nature*. 2012;486(7403):346–352.
75. Gluck S, et al. TP53 genomics predict higher clinical and pathologic tumor response in operable early-stage breast cancer treated with docetaxel-capecitabine ± trastuzumab. *Breast Cancer Res Treat*. 2012; 132(3):781–791.
76. Turashvili G, et al. Novel markers for differentiation of lobular and ductal invasive breast carcinomas by laser microdissection and microarray analysis. *BMC Cancer*. 2007;7:55.